CHALMERS
UNIVERSITY OF TECHNOLOGY

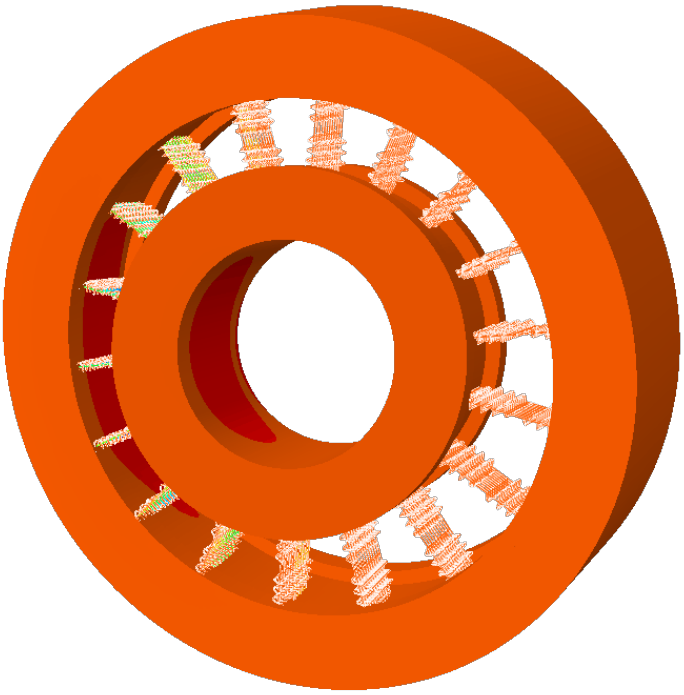

An Investigation of Finite Element Models of Roller Bearings

A summary of different studies on the effect of bearing size, meshes, spring density and roller-modelling on the stiffness of roller bearing models

Master's thesis in Applied Mechanics

RAMIN RAHANI

DEPARTMENT OF INDUSTRIAL AND MATERIALS SCIENCE
CHALMERS UNIVERSITY OF TECHNOLOGY
Gothenburg, Sweden 2021
www.chalmers.se

Master's thesis 2021

An Investigation of Finite Element Models of Roller Bearings

A summary of different studies on the effect of bearing size, meshes, spring density and roller-modelling on the stiffness of roller bearing models

RAMIN RAHANI

CHALMERS
UNIVERSITY OF TECHNOLOGY

Department of Industrial and Materials Science
Division of Material and Computational Mechanics
Chalmers University of Technology
Gothenburg, Sweden 2021

An Investigation of Finite Element Models of Roller Bearings
A summary of different studies on the effect of bearing size, meshes, spring density and roller-modelling on the stiffness of roller bearing models
RAMIN RAHANI

Supervisors: Sven Norberg, Jonas Koch, Volvo Group Trucks Technology
Examiner: Fredrik Larsson, Department of Industrial and Materials Science

Master's Thesis 2021
Department of Industrial and Materials Science
Division of Material and Computational Mechanics
Chalmers University of Technology
SE-412 96 Gothenburg
Telephone +46 31 772 1000

Cover: A cylindrical roller bearing visualized in Abaqus Viewer showing gap-elements and springs under radial load and misalignment.

Typeset in LaTeX
Printed by Chalmers Reproservice
Gothenburg, Sweden 2021

An investigation of finite element models of roller bearings
A summary of different studies on the effect of bearing size, meshes, spring density and roller-modelling on the stiffness of roller bearing models
RAMIN RAHANI
Department of Industrial and Materials Science
Chalmers University of Technology

Abstract

Increasing demands on the design of transmissions for heavy trucks include higher loads, longer lifetime and reduction of noise. To design gearboxes with aid of the finite element method it is important to obtain precise force transfer and thus accurate stress distribution close to a roller bearing seat. Therefore, stable and numerically accurate bearing models are necessary. The purpose of the thesis is to accurately describe the local or average behavior of roller bearings and to present finite element results of the required detail level close to the bearings. It entails calibration of bearing models with results from commercial bearing analysis tools. The objectives are to find improved ways to model the change from contact to play between the rollers and the rings, study stiffness of different bearing distribution models, investigate mesh-sensitivity and implement axial stiffness in the bearing models. The Abaqus finite element software is used to predict the behavior of roller bearings. The analysis includes modelling of bearings and execution of load steps. Matlab scripts are used to post-process the bearing models and evaluate them with bearing analysis tools. The commercial software Shaft and Bearing Analysis (SABR) is used to create bearing reference models. An optimization process is implemented with Matlab to automate the convergence process of SABR. The developed model with GAP-elements agrees with the reference model in the same way as the model using nonlinear springs. Bearing models with different distribution loads show increasing deformation as the ring thickness increases. For bearings of extreme sizes, it is found that small rollers are slightly more flexible and large rollers a bit stiffer. The mesh study demonstrates that the relative size difference between adjacent elements does not affect the stiffness. When the spring spacing is equal to or smaller than the element size, the bearing stiffness is not affected by the spring spacing or the element size. The deflection of the bearings is influenced by the axial play. Axial stiffness should be high and does not give a large contribution to the total deflection. The results from the Abaqus bearing models provide good accuracy to model pure radial, pure axial and a combination of radial and axial loads along with bearing misalignments.

Keywords: axial, radial, rings, roller bearing, springs, stiffness

Acknowledgements

I gratefully acknowledge and thank the support and guidance from my supervisors Sven Norberg and Jonas Koch at Volvo Group Trucks Technology, PE Driveline. Their expertise have helped and guided me throughout the entire thesis. Their insightful comments have driven me to refine my thinking and take my work to a higher level. My appreciation also extends to Maria Petersson for her assistance during my time at Volvo Group.

I would also like to express my deep gratitude to Professor Fredrik Larsson of the division of Material and Computational Mechanics, Department of Industrial and Materials Science at Chalmers University of Technology as the second reader and examiner of this thesis. I am gratefully indebted to his very valuable comments.

"Hay pintores que transforman el sol en una mancha amarilla, pero hay otros que con la ayuda de su arte y su inteligencia, transforman una mancha amarilla en sol."

- Pablo Picasso

Ramin Rahani, Gothenburg, June 2021

Nomenclature

Abbreviations

CAE	Computer-Aided Engineering
FE	Finite Element
GF	Growth Factors
GUI	Graphical User Interface
IR	Inner Ring
OR	Outer Ring
SABR	Shaft and Bearing Analysis Software

Greek Letters

τ	Dimensionless quantity to describe bearing thickness

Latin Letters

δ	Displacement of the inner ring with respect to the outer ring of the raceways
d	Minimum separation for the nodes that forms the gap
D_R	Roller diameter
F_x	Radial force
h	Opening of the gap
k	Load-deflection factor
n_x	Roller bearing exponent
Q	Roller-raceway deformation
t	Ring thickness
x	Node position

Contents

List of Figures

List of Tables

1
Introduction

1.1 Background

The computer-aided engineering (CAE) method Finite Elements Analysis (FEA) has become important to efficiently assess and model transmissions in motor vehicles. When designing gearboxes, developments such as sustaining more loads, having longer lifetime, and reducing noise are of great importance. In order to build good models for FEA, it is essential to understand how different loads are exerted on the gearbox and how those influence the gearbox [1].

In a typical gearbox, bearings are an important component since they transfer forces between other components such as shafts and housings. When implementing bearings in finite element models it becomes necessary to consider simplifications of the models since having large FE-models increases the computational requirements [2]. It is for example difficult to have a cylindrical roller bearing with all of its rollers in contact with the inner and outer rings in a static FE analysis, see Figure 1.1. That is, because it is hard to find a state of equilibrium for all of the rollers. By reducing the complexity of FE-models, less computational effort is needed, and thereby less time is required to numerically analyze the models. However, the models still need to be stable and give accurate results. This thesis treats the development of bearing models that are sufficiently detailed for accurate analysis while being still affordable to analyze.

1.1.1 Roller bearings

Roller bearings play a vital role when using applications that require extensive load supporting capacity. They are much stiffer and have a higher load capacity when compared to ball bearings of similar size. However, roller bearing assemblies are generally more expensive to manufacture than ball bearings of similar sizes [3]. Figures 1.2a, 1.2b and 1.2c show cross-sectional overviews of ball and roller bearings.

1.1.1.1 Cylindrical roller bearings

Cylindrical roller bearings are suitable for applications with high temperature, loads and rotational speed. The rings can be constructed with roller guiding flanges in order to support thrust load as displayed in Figure 1.2b. Rollers are crowned to avoid edge stresses and provide protection against misalignment. The bearings can be constructed with more than one roller row in order to carry greater radial-load and reduce skewness [3].

1.1.1.2 Needle roller bearings

Needle rollers have a substantially greater length than diameter compared to cylindrical rollers, see Figure 1.2c. As a result manufacturing accuracy is reduced because of the roller geometry which in turn increases the friction of the bearings. Usually, needle roller bearings are used in applications where radial space is limited. They are advantageous for designs that have extensive oscillations [3].

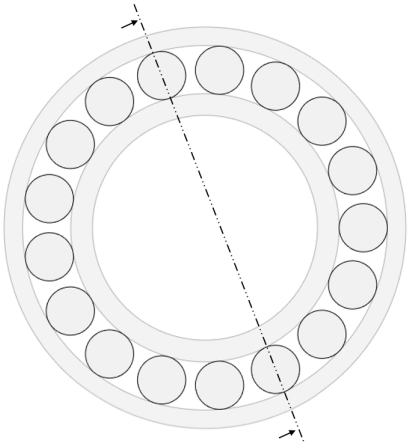

Figure 1.1: Axial view of a rolling bearing.

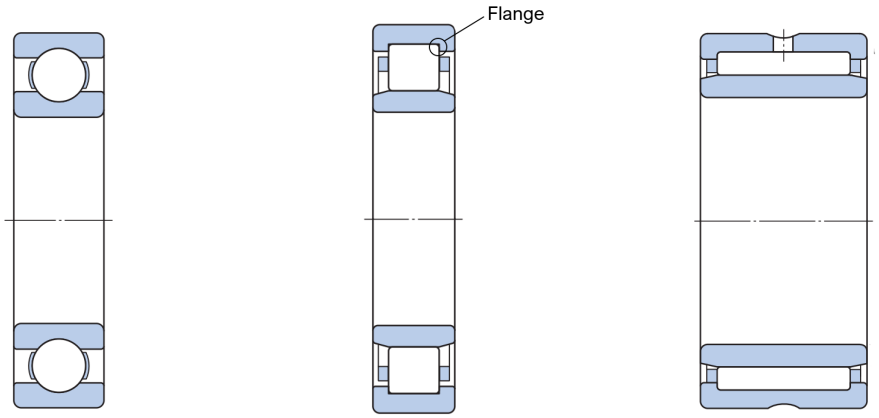

Figure 1.2: Illustration of different rolling bearing designs: a) Single row deep groove ball bearing. b) Single row cylindrical roller bearing. c) Single row needle roller bearing.

1.1.2 Lincoln bearing analysis tool

Lincoln is an in-house Matlab-based graphical user interface (GUI) from Volvo that is used as a tool to create Abaqus models of rolling bearings. The GUI consist of six-panel displays where each fulfills its purpose by a set of parameters that varies dependent on which bearing type that is selected, see Figure 1.3. Lincoln is able to model tapered, cylindrical and ball bearings. Needle bearings are treated as a special case of cylindrical bearings [4].

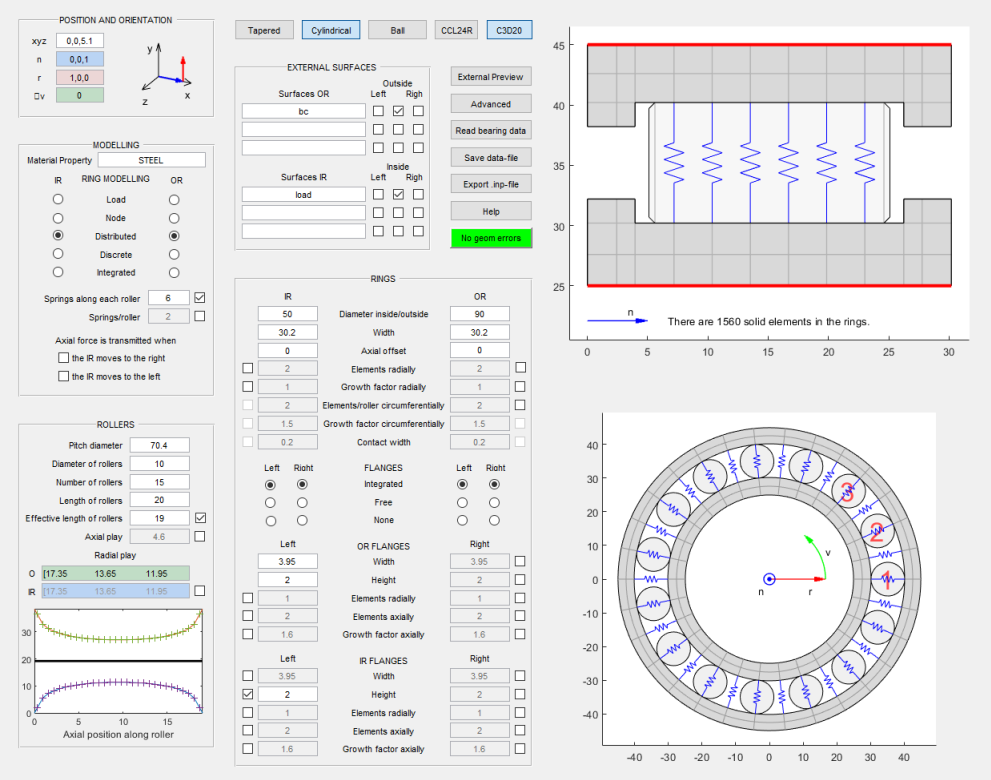

Figure 1.3: Lincoln is a Matlab (GUI) that is used as a tool to model bearings. The GUI is composed of six panels where each one fulfills its objective by a set of parameters that are described differently depending on the selected bearing type.

1.2 Aim and objectives

This thesis aims to develop models that are able to correctly describe the average or local behavior of bearings and provide finite element results of the desired detail level close to the bearings. This work involves creating roller bearing models as well as modifying and optimizing Matlab codes for the new implementations. Results from the models should be validated with results from dedicated commercial shaft and bearing analysis tools. The specific objectives are the following:

- Identify better ways to model the change from contact to play between the rollers and the rings. The new models should take less computational time than the present models.
- Investigate stiffness of integrated rings and observed difference between needle and roller bearings.
- Study mesh influence of discrete bearing models.
- Investigate the axial and combined radial and axial forces and possibly calibrate the model.

1.3 Limitations

Abaqus 2018 is in this thesis used as the main prediction of the behavior of bearings under given conditions.

The load-cases consist of combinations of forces (purely radial, purely axial or combined radial and axial loads) and misalignments in orthogonal and parallel directions, see Section 3.1 for more detail.

The inner and outer surfaces of the inner and outer rings are defined as rigid bodies in the models. Actual bearing rollers are not used in the study, instead the behavior of the rollers is replaced by elements coupled in series.

A complete bearing assembly with surrounding parts such as shaft and housing is not analyzed. The bearing model is only analyzed.

2

Theoretical Framework

This chapter provides the essential theory for the thesis. The theory of cylindrical roller bearing models is mostly based on the Lincoln bearing analysis tool from Volvo. A general discussion about gap-elements, effective clearance and roller stiffness is presented.

2.1 The cylindrical roller bearing models

The cylindrical roller bearing models in transmissions have certain characteristics that are fundamental in this thesis. A bearing model consists of an inner and an outer ring connected by springs. The springs represent cylindrical roller bodies. It is possible to specify the number of springs that model each roller axially, see Figure 2.1b. Every roller has a certain number of spring rows per roller circumferentially, see Figure 2.1a [4], [5].

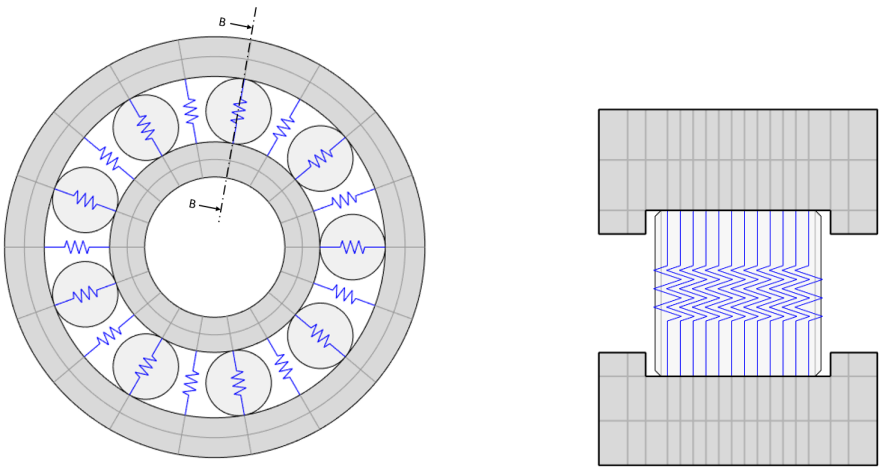

(a) Axial view of a cylindrical roller bearing model.

(b) Cross section of a roller bearing model.

Figure 2.1: A cylindrical bearing model from Lincoln. Inner and outer rings are connected by springs.

The springs are connected to the inner raceway and constrained in such a way that they remain perpendicular to the raceway. To enable rotation of the inner ring, the outer raceway and the outer nodes of the springs are connected by a contact, see Figure 2.2. The rollers have defined plays in radial and axial directions [5].

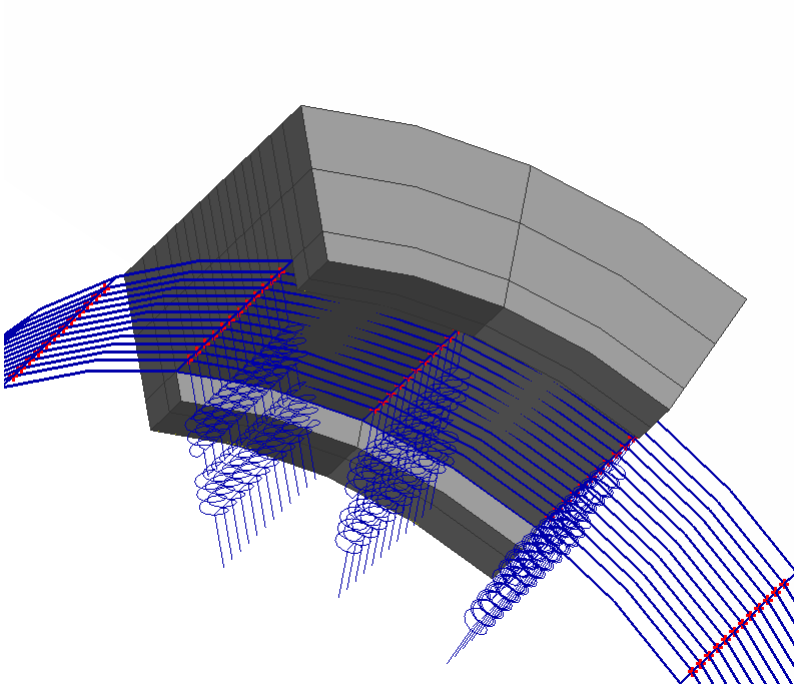

Figure 2.2: A contact definition (contact pair) is used to connect the outer raceway with the outer nodes of the springs.

The solid ring elements can be arranged as number of element layers in radial direction and number of elements between adjacent rollers circumferentially. The relative size differences between adjacent elements in radial and circumferential directions are scaled by growth factors [4].

2.1.1 Load distribution methods

The solid rings can be modelled with three different load distribution methods. The roller stiffness changes depending on the chosen model [4].

The first way is called *distributed*. The distributed model does not take the roller position into account; the force is smoothly distributed between the raceways under the applied load [4].

The second way is called *discrete*. The discrete model only transfers force between the rings at the positions where a roller is modelled [4]. The difference is illustrated in Figure 2.3.

In the third load bearing model, inner and outer rings are not created in Lincoln. Instead, only the springs are created in Lincoln and connected to existing geometry from other parts, see Figure 2.4 [4]. This way of assigning load is named *integrated* loading and is common for needle bearings, for instance between shafts and loose gear wheels.

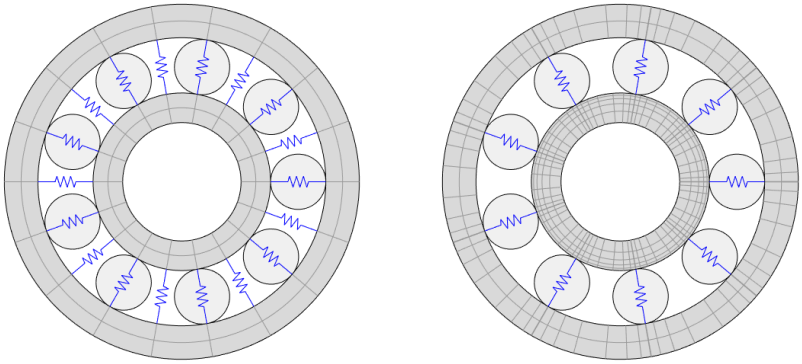

(a) Distributed loading **(b)** Discrete loading

Figure 2.3: a) The force load is distributed from the inner ring into elements of the outer ring. It can be seen as if the load is averaged. b) Line loads act along an element row on the outer ring when being exerted from the inner raceway. Such loads are applied locally and can therefore be used to understand what happens when the roller is in one specific position.

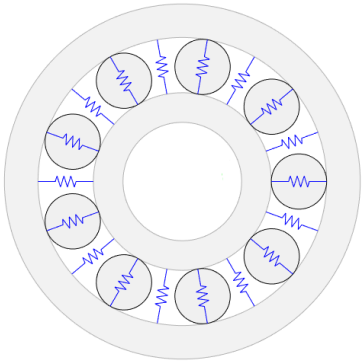

Figure 2.4: Integrated loading

The models differ when it comes to the number of spring rows circumferentially. Discrete loading treats rollers discretely and models each roller with a localized row of springs. As for distributed loading, the number of rows of springs for each roller is set by the user. The default is 2, which is the case in Figure 2.3a. In this way the roller stiffness is distributed over the ring. Distributed and discrete models differ also when it comes to the element size. The discrete model has more element layers in the radial direction below the bearing raceway and an increased number of elements in the circumferential direction for every roller [4].

2.2 Gap-element

Gap elements allow for contact between two nodes where the nodes can be in contact (closed gap) or separated (open gap), see Figure 2.5 [6].

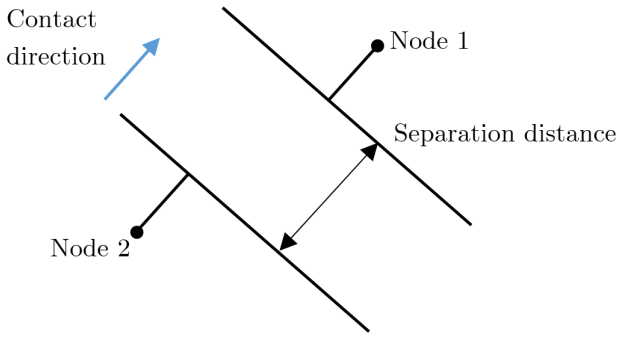

Figure 2.5: A gap element is defined by initial separation distance (clearance) between two nodes and the contact direction.

The behavior of GAPSPHER-elements in Abaqus models is defined by a minimum or maximum separation distance d between two nodes and current positions of the element's nodes. The contact situation can be thought of as two rigid spheres connected by the GAPSPHER element, see Figure 2.6.

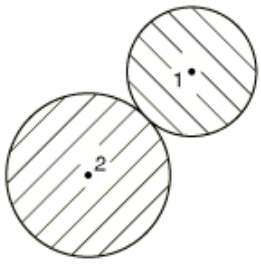

Figure 2.6: A contact between two rigid spheres along their external surfaces. The behavior of a GAPSPHER element is specified by the current positions of the element's nodes and the minimum or maximum separation distance between the nodes. The contact direction is defined by the current position of the nodes.

When the separation distance d is negative, an external contact is present between the elements in question. In this case, d is the minimum separation for the nodes that form the gap. When the gap is closed, the two nodes are in the same location. The opening of the gap h is for this case defined as

$$h = \left|\boldsymbol{x^2} - \boldsymbol{x^1}\right| - |d| \tag{2.1}$$

where $\boldsymbol{x}$ is the node position. The value $d = 0$ is not allowed since it would make the distance between the nodes to be zero [6].

2.3 Effective clearance

The effective clearance is the relative movement of inner and outer rings being at their operating temperature, see Figure 2.7. Effective clearance affects the load distribution in a bearing which in turn affects the bearing life. Noise and vibration are also influenced by this parameter [7], [8].

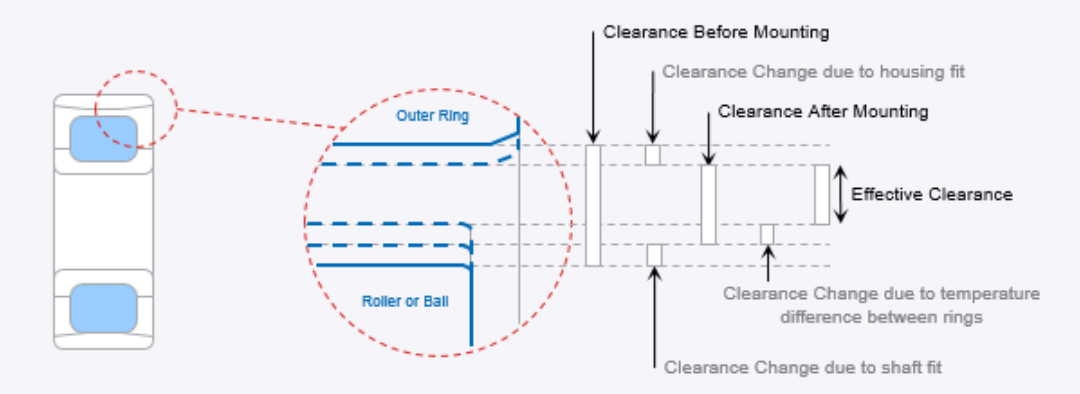

Figure 2.7: Internal diametrical clearance for a rolling bearing. Effective clearance: clearance of the bearing being at its operating temperature without taking elastic deformation into account.

2.4 Stiffness relations of rollers

Claesson [5] investigated from various sources the expressions to calculate the roller-raceway deformation (roller load) Q for a roller-raceway contact as:

$$Q = k\delta^n \tag{2.2}$$

where δ is the displacement of the inner ring with respect to the outer ring of the raceways, n the roller bearing exponent and k the load-deflection factor. Due to equilibrium, the roller load Q is equal in the inner and outer ring. The load-deflection factor k can be expressed as:

$$k = \left[\frac{1}{\left(\frac{1}{k_i}\right)^{\frac{1}{n}} + \left(\frac{1}{k_o}\right)^{\frac{1}{n}}} \right]^n \tag{2.3}$$

where k_i is the load-deflection factor of the inner ring and k_o the load-deflection factor of the outer ring [5].

The roller-raceway deformation Q can be expressed as:

$$Q = C \left(\frac{L}{L_0}\right)^{n_1} \left(\frac{D}{D_0}\right)^{n_2} \left(\frac{\delta}{\delta_0}\right)^{n_3} \tag{2.4}$$

where L is the effective length of the roller. It is related to the load-deflection factor k. D is the roller diameter. L_0, D_0 and δ_0 are used as normalization parameters. The constant C and exponents n_1, n_2 and n_3 are based on experiments and theories from different authors [5].

3
Method

Lincoln bearing models are evaluated by a number of load cases that are analyzed by both the commercial software SABR and Lincoln generated Abaqus models. Results from SABR are treated as reference to evaluate Abaqus bearings using Matlab scripts.

3.1 Load cases

A load-case is a combination of forces acting on the bearing and bearing misalignments. Forces can consist of only radial, axial or combined radial and axial loads [3]. The radial force acts perpendicular to the shaft. The x-axis represents the radial direction, y-axis the orthogonal direction and z-axis the axial direction. The axial force acts along the shaft. Bearing misalignment occurs when the inner ring is not rotationally aligned with the outer ring [3]. Orthogonal and parallel misalignments are considered here. Orthogonal misalignment is a result of the inner ring tilting around the y-axis which is orthogonal to the load vector acting in the x-direction, see Figure 3.1b. With parallel misalignment the inner ring is tilted around the x-axis, see Figure 3.1c. Since the load vector is applied in x-direction it becomes parallel to the misalignment.

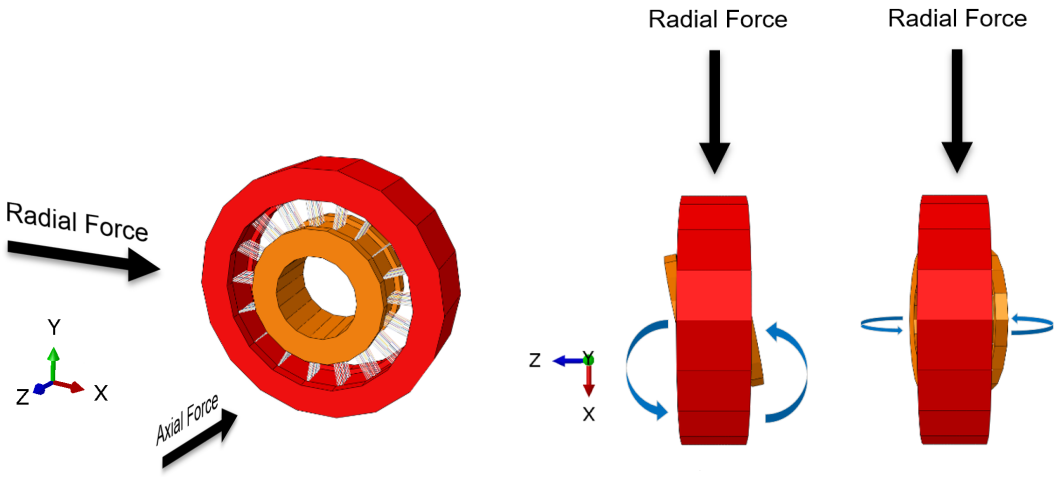

(a) Isometric view.

(b) Right view during orthogonal misalignment.

(c) Right view during parallel misalignment.

Figure 3.1: Cylindrical roller bearing in initial and misaligned conditions.

In most cases only radial force is applied. Four force levels are chosen based on the dynamic load rating of the bearing under analysis. The dynamic load rating is used to calculate rating life for bearings that rotate under load. The load is assumed as constant and purely radial during its rating life [9]. The force levels are gradually increased where the highest load is approximately half of the dynamic load rating of the bearing. For these four loads nine different combinations of misalignments are used, see Table 3.1. The values are based on actual bearing misalignments in current Volvo applications. Each misalignment step consists of a parallel and orthogonal misalignment. The methods presented later in this chapter are shaped and evaluated around these load-cases.

Table 3.1: The combined misalignments that are used with respective radial load.

Misalignment step	1	2	3	4	5	6	7	8	9
Parallel [mrad]	0	0	0	1	1	1	3	3	3
Orthogonal [mrad]	0	1	3	0	1	3	0	1	3

3.2 Shaft and bearing analysis software

Shaft and Bearing Analysis Software, abbreviated SABR, is a commercial software from Ricardo PLC that is used to model transmission systems and their components. The software package carries out gear, shaft and bearing analysis to determine forces and deformations. These are used to determine bearing (and gear) life and misalignments. Solver algorithms are based on standardized bearing calculations [7].

SABR based results are in this thesis used as reference for Lincoln bearing models. To obtain the results a SABR model was created, see Figure 3.2.

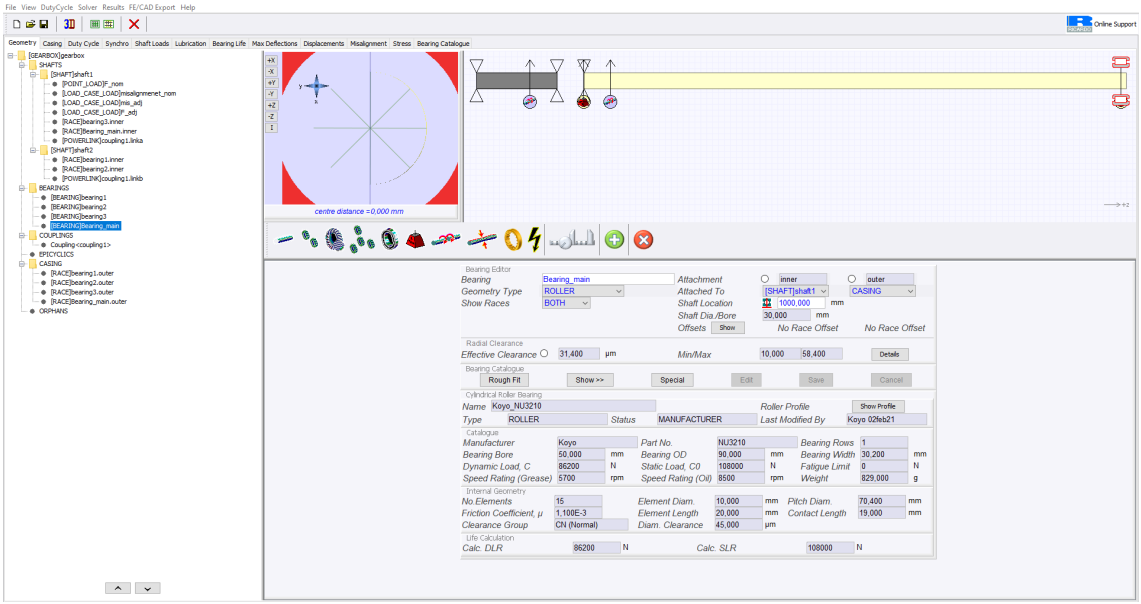

Figure 3.2: SABR Model Reference.

It consists of two shafts where the left one, shaft 2, has a length of 150 mm and the

right one, shaft 1, a length of 1010 mm. A coupling connects the shafts and makes them rotate together. Shaft 1 has the cylindrical roller bearing of interest specified on the right end and a linear bearing on the left end. The linear bearing supports the shaft with a linear stiffness to ground. Shaft 2 has two linear bearings defined on its respective ends.

Two types of loads are used in this system. 'Simple point load' is the first one that represents a fixed load applied on a shaft. It is the same for all load cases in a SABR file. The second type is 'load case load' where the load is specified individually for each load case in the file [7].

One SABR file is created for the load case with the same bearing load. This load is modelled with a simple-point-load on the right end of shaft 1. A load-case-load on the left end is used to impose misalignments. The stiffness of the left hand linear bearing is 1000 N/mm. This gives a bearing misalignment of 1 mrad when applying 1000 N in the radial direction. The two discussed shaft loads are here considered as 'nominal loads' since their values reflect the wanted loads and misalignments. However, the resulting bearing load and misalignment are not exactly as wanted. This is due to the deformation of the roller bearing and the redistribution of the forces when the bearing is misaligned.

3.2.1 Load-case example

The iteration process for a load-case example is described here. Nominal loads for this case are presented in Table 3.2. As noted, the radial load acts in the x-direction. The example has a radial load of 30 kN and an orthogonal misalignment of 1 mrad.

Table 3.2: Nominal loads for the load-case example.

Simple Point Load (F_x)	30000 N
Misalignment Load-Case-Load (F_x)	-1000 N

It is necessary to introduce adjusting loads and iterate to compensate for the redistribution of the forces and hence obtain the desired result. A load-case-load for respective nominal shaft load was added. These additional loads are designated as 'adjusting loads' since they are variable. Figure 3.3 illustrates the model in this example.

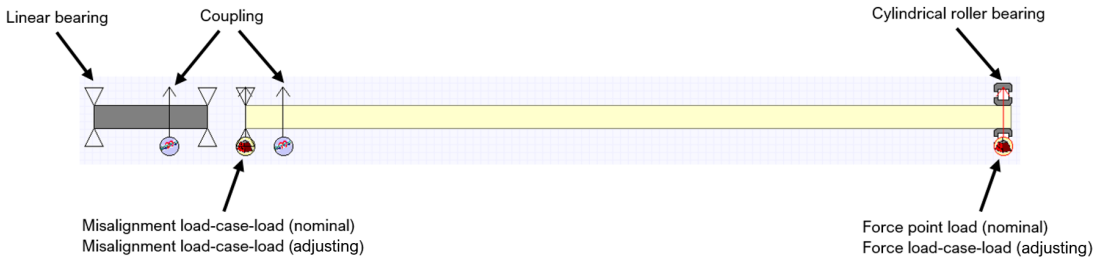

Figure 3.3: Geometry model of example.

Once the problem was defined by the foregoing steps, the results were computed by SABR. Initial SABR results, which include reaction loads and displacements for the load case, are shown in Figure 3.4. The point load came to be 29991.2 N which gave an error of 8.8 N. The orthogonal misalignment error was 0.061 mrad. The load-case-load adjusters were used to correct these errors. An x-component of the adjuster for the point load of 8.8 N was added. A corresponding adjustment was done for the misalignment with 61 N.

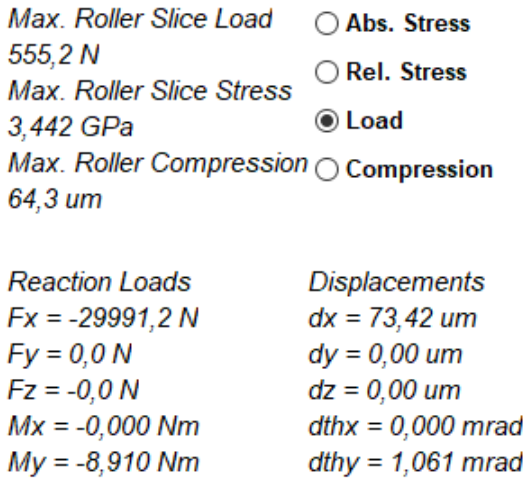

Figure 3.4: SABR Rolling Element Loads: *First* results.

The first iteration gave improved results, as shown in Figure 3.5. Despite this, small deviations still remained. An additional iteration was needed to get error free results, see Table 3.3.

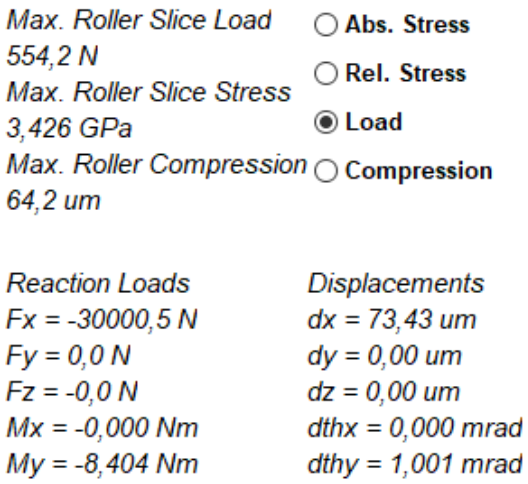

Figure 3.5: SABR Rolling Element Loads: *Second* results.

Table 3.3: Reaction load and misalignment errors with their adjusters in x-direction through all iterations in the example.

Iteration	Point Error	Misalign. Error	Point Adj. (F_x)	Misalign. Adj. (F_x)
0	8.8 N	0.061 mrad	0.0 N	0.0 N
1	0.5 N	0.001 mrad	8.8 N	61 N
2	0.0 N	0.0 mrad	8.3 N	62 N

It can be seen from this example that it is required to iterate to get the target load and misalignment. Performing the adjustment manually is ineffective and becomes time-consuming when having many load-cases. This was seen as a major drawback in SABR. A programming process was therefore employed to automate the converging process.

3.2.2 Automation of SABR convergence process

Programming methods offer an effective way to automate project tasks. To begin this process, it was first required to systematize defined load case names. Every load case includes radial load, axial load, parallel misalignment and orthogonal misalignment as discussed previously in Section 3.1. The load-case names represent nominal loads as previously defined. It is possible to combine radial and axial loads. An example of such a load-case is pw_r30000N_a5000N_vp1_vo3 where 30000 is the radial force (N), 5000 the axial force (N), 1 parallel misalignment (mrad) and 3 orthogonal misalignment (mrad).

The sequences of the created Matlab algorithm are illustrated as a flowchart diagram in Figure 3.6.

The first iteration of the model with nominal loads generates results saved in a SABR (*.GBX*) file. Additional results are written to a comma-separated values (*.CSV*) file [7]. The GBX and CSV files with matching names are used as input in Matlab, once the script is started. The extraction is initiated by locating the duty cycle section in the CSV file and thereafter collect load cases into cell arrays. A major issue in this process was that each file has data sorted in a specific order. It was necessary to find and store both load-cases of the files since each file has them differently ordered. It was also necessary to assign relationships between GBX and CSV in order to determine the difference between nominal and actual misalignments.

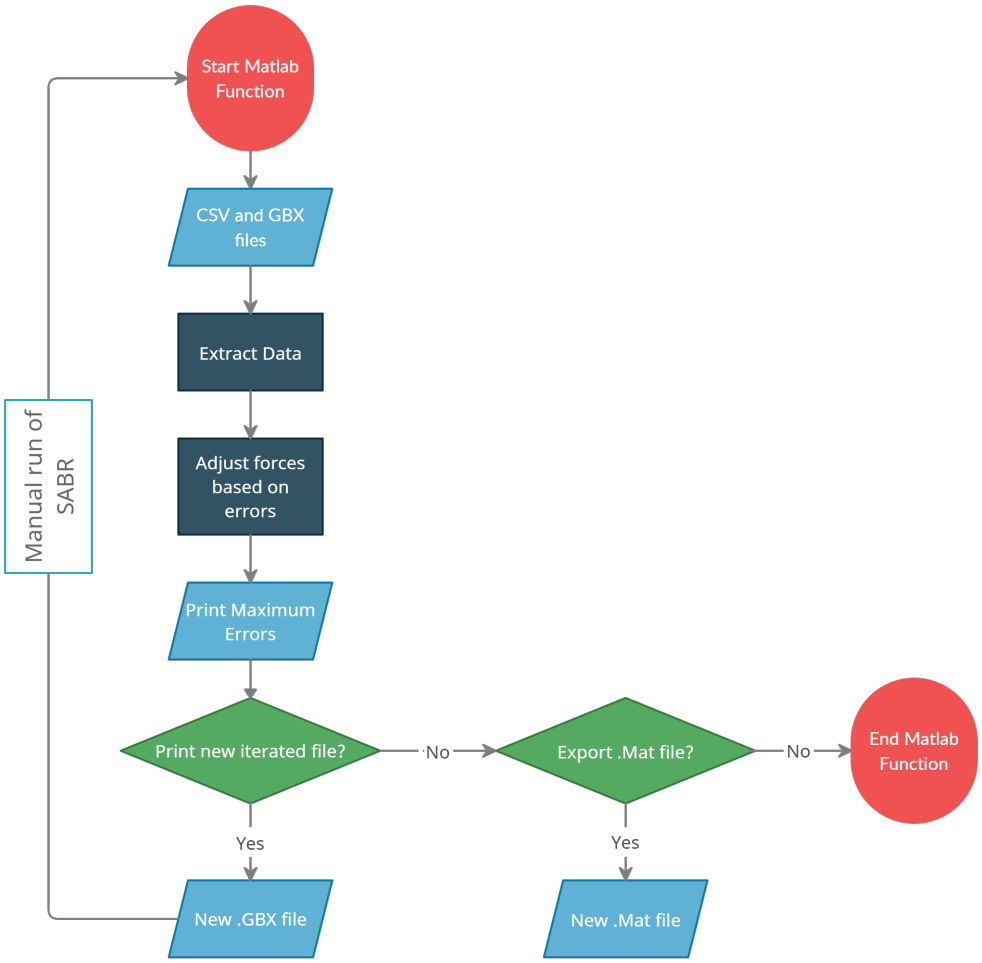

Figure 3.6: The Matlab algorithm represented by a flowchart diagram.

Bearing loads include reaction forces and reaction moments. To locate bearing loads from the CSV file, the rows of the bearing section that contains these results are identified. Nominal load-case forces are extracted from the load case names and stored into matrices. Each column corresponds to each force component for every load-case. A similar matrix is created for the reaction moments, where columns correspond to reaction moments in orthogonal and parallel directions.

The solver-results section in the GBX file is located and displacements and misalignments are extracted as arrays. Displacement components for every load case are from this array stored in one matrix and misalignments in a similar one. The next step was to extract nominal forces (radial and axial) for every load case from the GBX file.

The resulting load-case forces from the CSV file are subtracted from the nominal forces. The difference is called errors. After that, the current values of the adjusting forces are extracted from the GBX file and stored in a matrix. Errors between nominal and actual misalignments are computed. The adjustment process is started by computing new adjusting forces and misalignments. The adjusting forces are then updated with the computed errors.

To summarize the process:

1. The errors of the radial and axial forces are computed.
2. The errors of the misalignments are computed.
3. The force adjusters are modified with the errors computed in 1 and 2.

Maximum error values are at this stage printed in the Matlab command window to give the user an estimate of the convergence residual. The user can then make a decision to either print an updated GBX file for another loop in SABR, export a MAT file containing results for post-processing purposes or end the script. If new GBX file is chosen, a new file will be printed with the same name but incremented to indicate a new iteration. By choosing to export, a MAT file is created containing a matrix with displacements and moments for every load-case. The iterative solution procedure was usually repeated several times in order to get satisfying results. MAT files were mainly exported to validate FE results.

3.3 Finite element analysis with Abaqus

The finite element method using Abaqus 2018 is in this thesis used as the fundamental prediction of how bearing assemblies behave under given conditions. FE analysis generally starts with a pre-processing phase that creates input files containing an FE representation of the bearing. Such files are hereafter referred to as 'base-geometry files'. Two main approaches are used to create base-geometry files. Complete base-geometry files exported from Lincoln is one way. The other method consists of using Lincoln in combination with a Matlab function. In the latter method, the spring definitions are removed from Lincoln's output file and replaced by a parameterized Matlab function. Additional Abaqus constraints are needed in order to process the input file. These consist of material definition (see Table 3.4), reference nodes, coupling constraints and contact definitions [6].

Reference nodes located at the center of the bearing are connected with the rings using kinematic couplings. The couplings connect the inner ring's inner surface and the outer ring's outer surface rigidly to their respective reference node. The reference node can with this control every constraint which makes it easy to prescribe forces and movements. A contact pair is used to connect the outer nodes of the springs representing the rollers, with the outer raceway surface. To prevent separation between the contacts, it is required to add a surface interaction property with no separation [6].

Table 3.4: Material definition for elements in the rings.

Material	steel
Elastic Modulus [MPa]	210000
Poisson's ratio	0.3

In order to process the model, Abaqus analysis steps must be defined. This is done by a scripted file that defines the analysis steps with the previously mentioned combination of forces and misalignments. Before executing the actual load cases it

is required to initialize the contacts with displacements in the direction of the loads. The aim is to close the play remaining between the rollers and rings. The relevant results from each load case are exported to a (*.dat*) file that is later on used in the processing-phase, see Section 3.4 [6].

3.4 Post-processing with Matlab

The last stage in the FE-process is to calibrate the Lincoln model with results from reference models.

Separate Matlab functions are used to extract results from the DAT and MAT files. The functions are in turn used in a script to create calibration plots. These plots are created to summarize the results for different misalignments and different forces. The misalignment steps are defined on the y-axis and the forces on the x-axis. Bearing models are differentiated by colors, with the SABR reference data usually shown in blue. Offsets are used between the models to easier distinguish differences. Figure 3.7 exemplifies this by zooming in on a single load case.

The outcomes from each load-case consist of displacements and reaction moments. Solid lines represent displacements in axial and radial directions as seen in Figure 3.7a. Striped lines represent reaction moments in orthogonal and parallel directions, see Figure 3.7b. The reaction moments (striped lines) are connected to the end of the displacements (solid lines). This is done to simplify the comparison. To scale displacements and moments, in order to enhance the visibility, scale factors are defined in the script.

The post-processing is concluded by observing all load-cases as seen in Figure 3.8. In these examples, the bearing models are in agreement with the reference which is desirable.

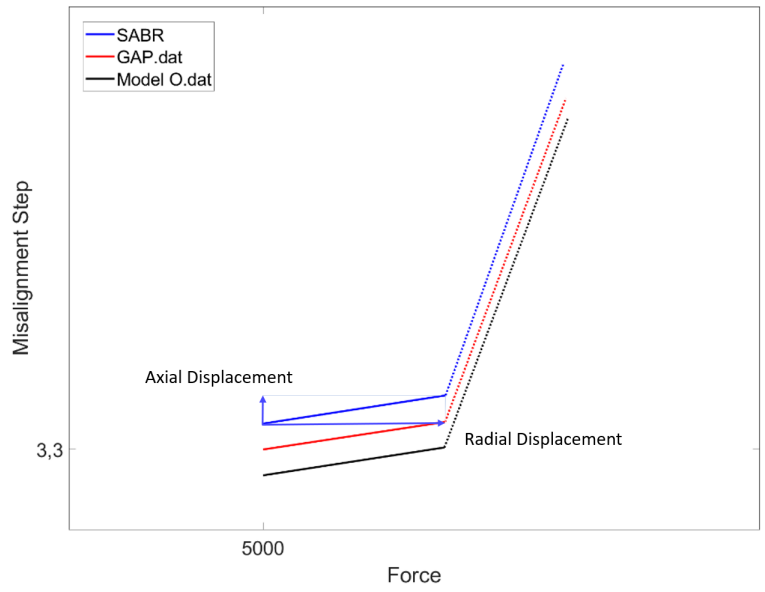

(a) Displacements in axial and radial direction.

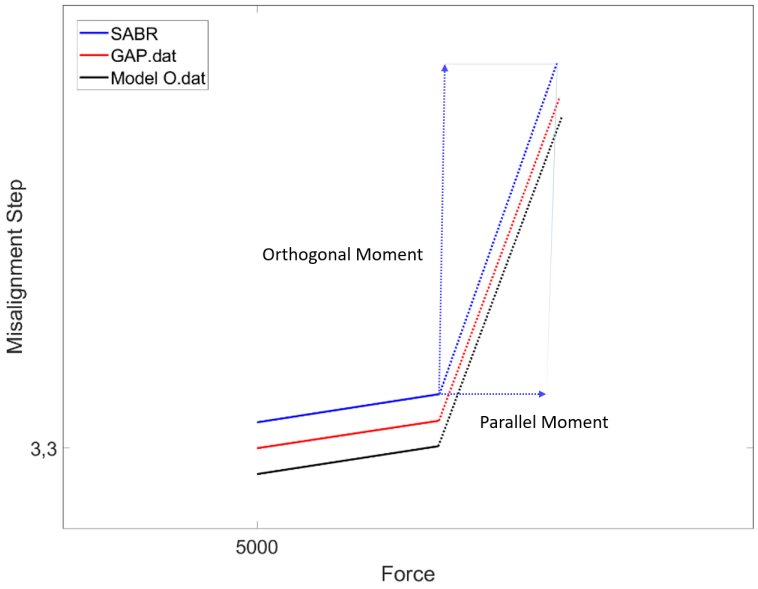

(b) Reaction moments in orthogonal and parallel direction.

Figure 3.7: Displacements and reaction moments from three different bearing models, oriented for parallel and orthogonal misalignment of 3 mrad for 5000 N radial load.

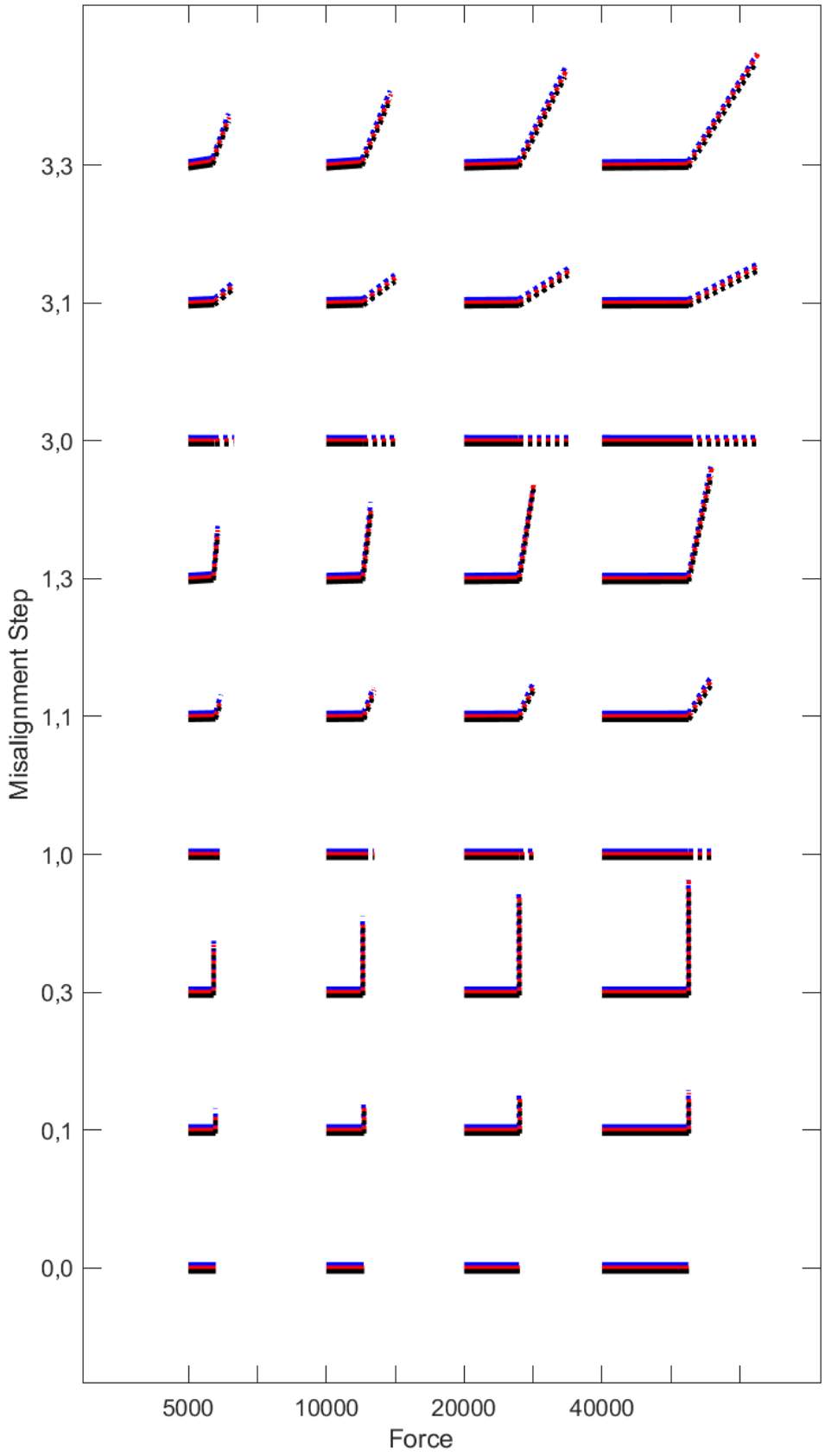

Figure 3.8: Displacement and reaction moments, oriented for nine misalignments and four radial loads.

4
Results

This chapter presents the specific investigations that were performed and their results. The original objectives are discussed in the next chapter based on the investigations presented here. The investigations consist of:

- Replacement of non-linear springs with gap elements in roller-modelling
- Simplification of discrete bearing model
- Investigation of the effect of ring thickness on bearing deflection
- Analysis of bearings with extreme size
- Mesh study of discrete bearing model
- Investigation of spring density and mesh size for integrated bearing models
- Investigation of axial forces for distributed bearing models.

4.1 Replacement of non-linear springs with gap elements in roller-modelling

With the current bearing model, large FE analyzes have been unstable and slow. The spring elements of the rollers in the model are the reason for this setback.

Model O implements non-linear spring elements which facilitate both opening and closing of the roller raceway contacts as well as allowing for the stiffness to change as the springs deform. Model O is shown in Figure 4.1, here visualized in the preprocessor tool ANSA.

Figure 4.2 illustrates the force-deformation relation for the springs of Model O. The contact section of the curve is located left of the transition kink. On the right side, there is a small tensile force while there is no contact. This was early on determined as the main weak point of the model. It appears when the roller loses contact with the raceway. The iterative solver has difficulties finding solutions close to the sharp transition.

The aim of this study was to find an option that makes the behavior of the roller model more efficient by avoiding this abrupt shift of the stiffness.

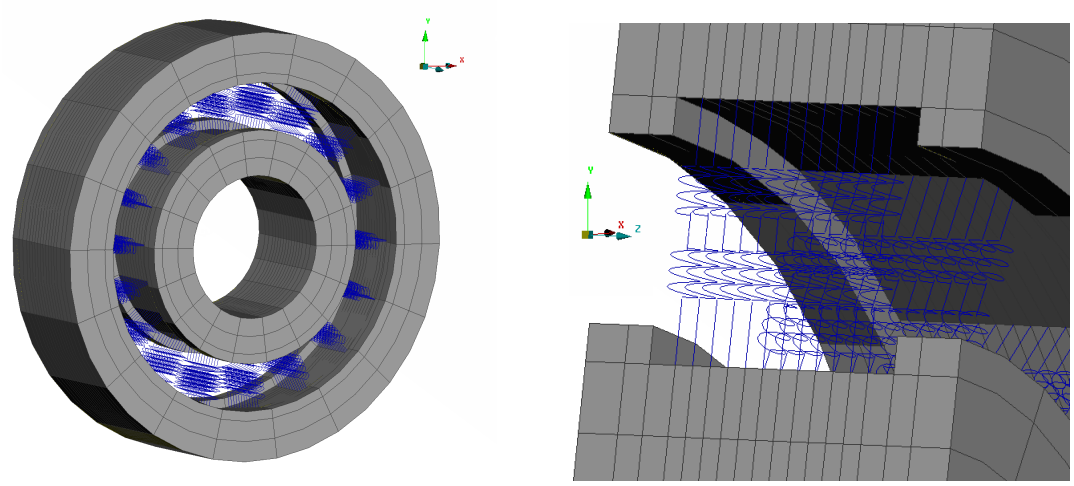

(a) Bearing Model O consists of 18 rollers and two solid rings. Each roller is constructed by spring elements in a row.

(b) Cross section of the bearing showing 12 connecting inner and outer spring elements distributed of each roller. This represents the behavior of each cylindrical roller.

Figure 4.1: Model O

Figure 4.2: Nonlinear stiffness for Model O (blue curve). The curve takes a sudden turn and becomes non-smooth before the force becomes constant. It appears when the roller loses contact. The nominal gap-element (red curve) has a 90 degree kink.

Gap-elements were selected as replacement for the non-linear springs on the basis of their ability to model opening and closing of contacts efficiently [6]. The default behavior of gap-elements is defined in Abaqus as a 90 degree kink on the force-deformation plot. The default stiffness curve is shown in Figure 4.2. However, it is possible to define a non-linear stiffness behavior for the gap-element. To keep the non-linear stiffness, the compressed part of the stiffness curve in Figure 4.2 is implemented. In other words, the transition is handled by the gap element. The kept non-linear stiffness is a way of modifying the gap element.

Different gap-elements with specific contact definitions are available in ABAQUS. Spherical gap (GAPSPHER) elements are chosen since the contact direction is arbitrary in space, i.e the inner ring has to be able to rotate. In order to add stiffness into the gap elements it was necessary to define a surface behavior with a force-deformation table [6].

A bearing has play between the raceways and rollers. The rollers are barrel-shaped to avoid excessive load on the corners. Therefore every gap element is given a play that decreases gradually from outermost until the midmost elements, see Figure 4.3.

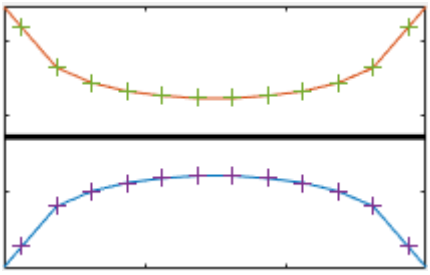

Figure 4.3: Radial play along a roller for inner and outer rings.

Once the new model was complete, computed results were compared to Model O. The first step in this process was to study and compare output files. To determine the number of increments that Abaqus used for each step and if cutbacks occurred, status (*.sta*) files from the analyzes were studied. Once convergence was confirmed, output database files that contain the analysis results were imported into Abaqus Viewer for further investigation [6]. Here it was visually analyzed if elements behaved as expected during each step and frame.

Figure 4.4 compares the force distribution in the spring and gap elements under the radial load of 20 [kN] in the first misalignment step. No force difference greater than this illustration was found by comparing other load cases.

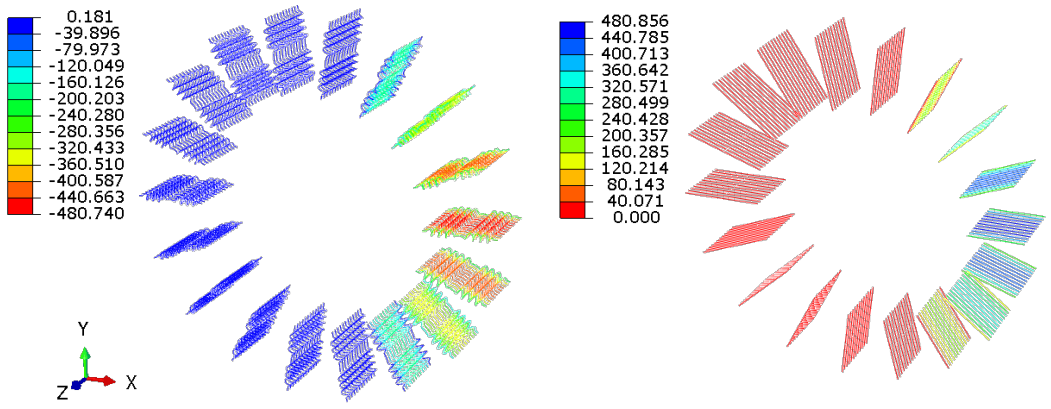

(a) **(b)**

Figure 4.4: a) Model O with displayed non linear springs under radial load of 20 [kN] in the first misalignment step. b) The developed model with displayed gap elements under radial load of 20 [kN] in the first misalignment step. Note that the sign convention for spring and gap elements are inverted.

The final stage of this process was to compare the new model with Model O and SABR. Results involving reaction moments and displacements from SABR and Model O were used to evaluate the developed bearing model, see Figure 4.5. It could be seen that the developed gap-model demonstrates matching deflection and reaction moments with Model O. Closer inspection showed however that there exist modest moment and stiffness differences between especially the Lincoln models and SABR. The reference model SABR showed slightly higher stiffness than the other models.

This study confirms that the developed model with GAP-elements agrees with reference (SABR) in the same way as the model using nonlinear springs (Model O).

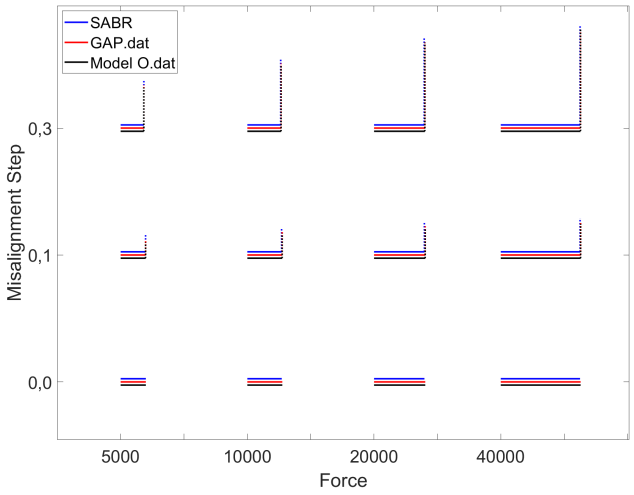

(a)

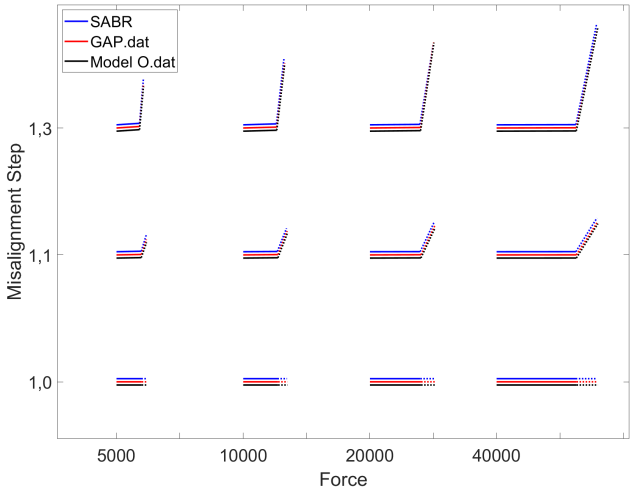

(b)

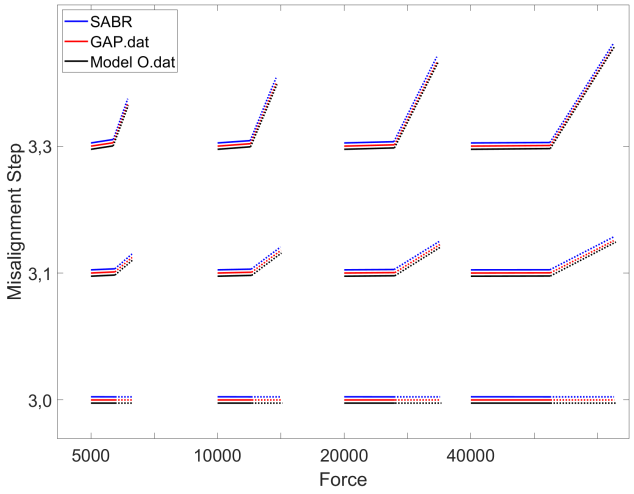

(c)

Figure 4.5: Displacements and reaction moments for different misalignment steps a) 1-3, b) 4-6 and c) 7-9 and different radial loads.

4.2 Simplification of discrete bearing models

The discrete bearing models have inner and outer rings with varying element sizes in radial and circumferential directions. In the circumferential direction, very thin elements appear underneath the springs modelling the rollers, see Figure 4.6. They represent the width of the roller-raceway contact. The springs are connected to the middle node of the elements. The high aspect ratio of these elements causes issues with the stability of the analysis. The investigation was if these elements could be removed without compromising the results.

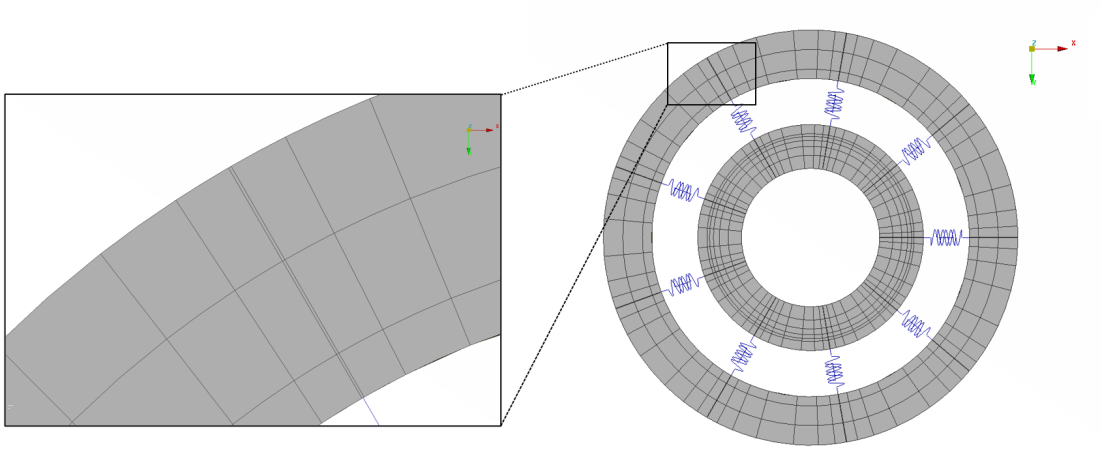

Figure 4.6: Discrete bearing model with very thin ring elements.

The thin elements were removed by increasing the size of adjacent elements. The springs were after the modification connected to the corner node of the elements. Figure 4.7 shows that the results for the new simplified model are close to those for the original model. No problems are expected with this simplification.

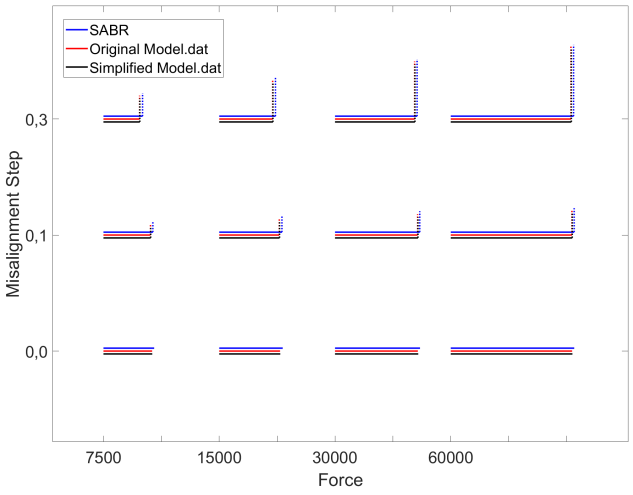

(a)

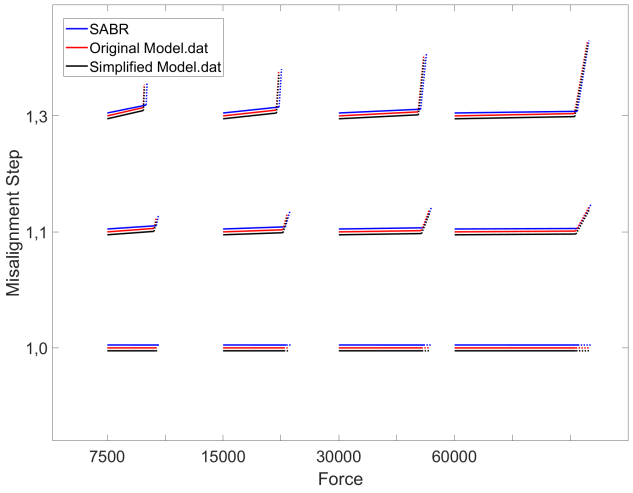

(b)

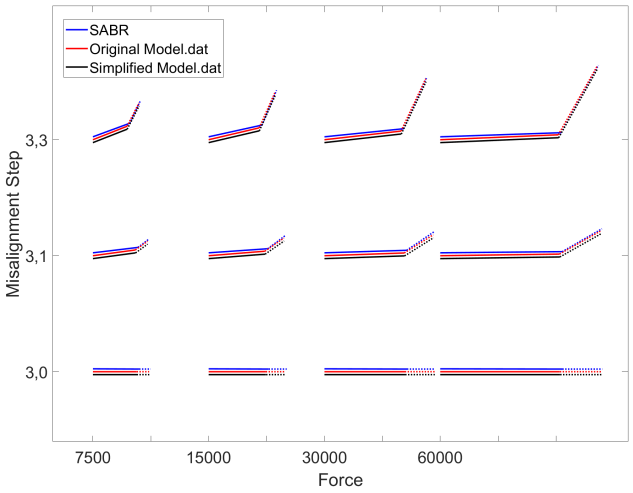

(c)

Figure 4.7: Displacements and reaction moments for different misalignment steps a) 1-3, b) 4-6 and c) 7-9 and different radial loads.

4.3 Investigation of the effect of ring thickness on bearing deflection

The nominal models consist of two different cylindrical roller bearings. 'Nominal' indicates that the geometries of the bearings are unmodified . Table 4.1 displays the base dimensions of the nominal bearings. Two finite element models were generated in Lincoln for each nominal bearing. The load distribution methods distributed and discrete are used for both bearings.

Table 4.1: The base dimensions of the two nominal roller bearings.

Name	Koyo_Cylindrical_50x90	Koyo_Cylindrical_30x90
Bearing Bore [mm]	50.00	30.00
Bearing OD [mm]	90.00	90.00
Bearing Width [mm]	30.20	23.50
No. Elements	15	9
Element Diam. [mm]	10	14
Pitch Diam. [mm]	70.40	59.00
Element Length [mm]	20.00	14.00
Contact Length [mm]	19.00	13.00
Diam. Clearance [μm]	45.00	32.50
Effective Clearance [μm]	31.40	20.50

After establishing the nominal bearing models, additional models with the same roller geometry but varying ring thickness were created. Figure 4.8 compares the difference.

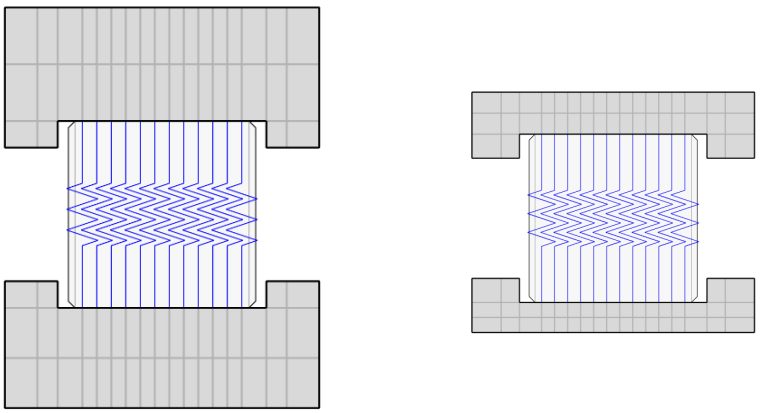

(a) Bore diameter 30 mm, Outer diameter 90 mm

(b) Bore diameter 40 mm, Outer diameter 80 mm

Figure 4.8: Distributed bearing models with different ring thicknesses.

Outer and inner rings for each bearing have the same thickness, the same changes are done in the inner as in the outer ring diameter. The analyzed ring thicknesses of the bearings are described by the dimensionless quantity

$$\tau = \frac{t}{D_R} \tag{4.1}$$

where t is the ring thickness and D_R the roller diameter. The scalar quantity τ was varied in steps of approximately 0.25 in order to get an even but dense distance between the new bearings. The chosen bearing models with modified rings are illustrated in Table 4.2. They are specified with inner (bore) diameter times outer diameter. A wide range of ring sizes are created for each of the bearings.

Table 4.2: Modified rings that are characterized by outer and inner (bore) ring diameter, e.g. 50x90. The columns are sorted by ascending ring thicknesses t [mm].

Modified Rings	
Koyo_Cylindrical_50x90 (t=5)	Koyo_Cylindrical_30x90 (t=8)
56x84 (t=2)	44x76 (t=1)
53x87 (t=3.5)	42x78 (t=2)
47x93 (t=6.5)	41x79 (t=2.5)
40x100 (t=10)	37x83 (t=4.5)
33x107 (t=13.5)	34x86 (t=6)
30x110 (t=15)	23x97 (t=11.5)
23x117 (t=18.5)	16x104 (t=15)
20x120 (t=20)	12x108 (t=17)
17x123 (t=21.5)	10x110 (t=18)
10x130 (t=25)	5x116 (t=20.75)
5x135 (t=27.5)	2x118 (t=22)

Results are plotted in Figure 4.9. Since only pure radial force is applied, the bearings are only displaced in the x-direction with no misalignment, cf. Section 3.1. Apart from the Lincoln bearings, reference models from SABR are included with the same sizes, as shown in the figure. Vertical grey lines indicate the nominal bearings.

It can be seen that the discrete and distributed bearing models behave in a similar way except for the very thin bearing rings. Deformation increases as the rings become thicker. In the discrete model only a small part of the rings are loaded where as for the distributed models, the load is distributed over a larger area. The bearings from SABR have step-wise deflection change. It was discovered that this was caused by changing the ring thickness in SABR. This caused SABR to also change the effective clearance of the bearing depending on the shaft and seat diameter.

From Table 4.2, a couple of rings for each bearing were selected and analyzed with the same effective clearance as the nominal bearings, cf. Table 4.1. The results of this analysis are shown in Figure 4.10. Curve fitting is used to fit each data set with different ring thicknesses (data points). As expected, SABR does not show any dependency between stiffness and ring dimension.

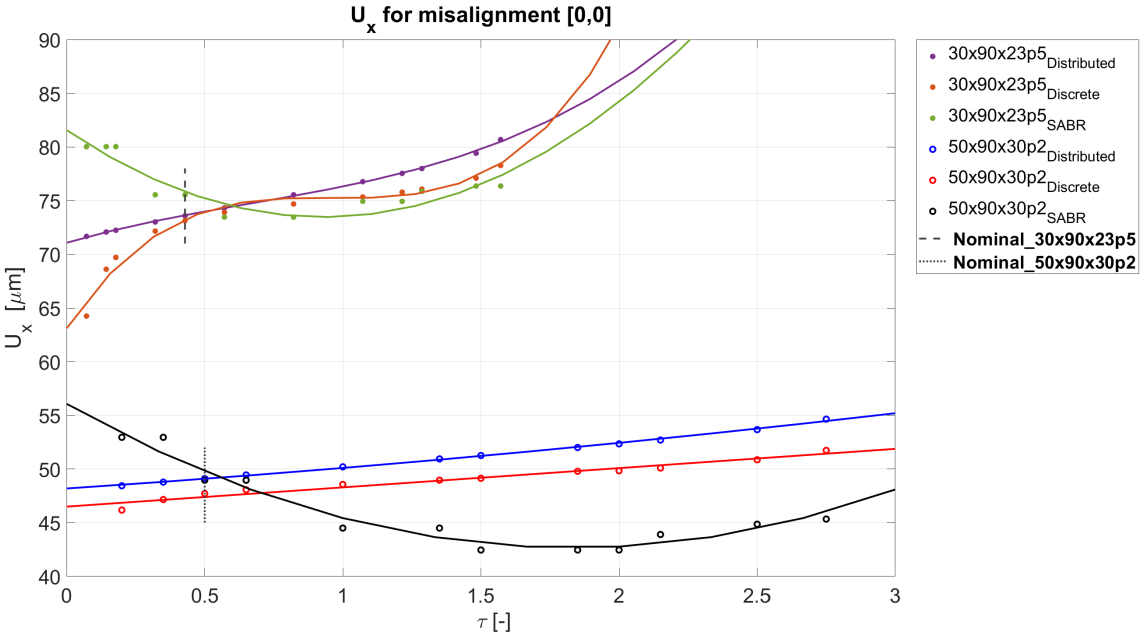

Figure 4.9: Deformation plotted as a function of $\tau = t/D_R$ for modified bearing models of Koyo_Cylindrical_50x90, Koyo_Cylindrical_30x90 and their respective SABR reference models. The bearings from SABR have step-wise deflection change since the effective clearance is different for each modified ring thickness.

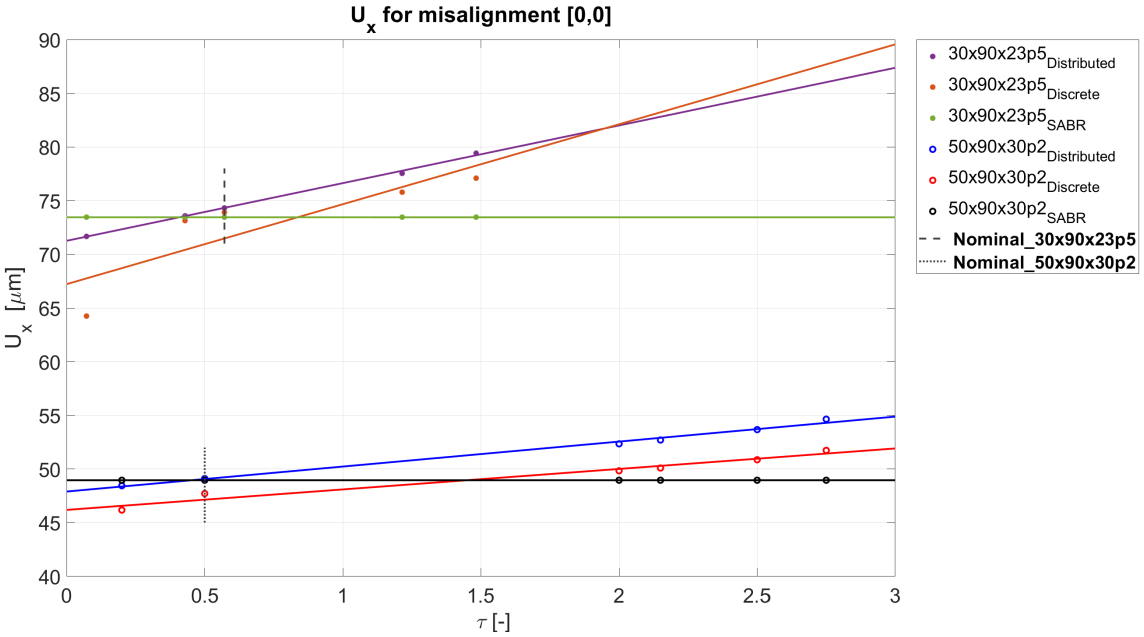

Figure 4.10: Deformation plotted as a function of $\tau = t/D_R$ for modified bearing models of Koyo_Cylindrical_50x90, Koyo_Cylindrical_30x90 and their respective SABR reference models. SABR bearings are analyzed with nominal effective clearance.

4.4 Analysis of bearings with extreme size

This study is established to analyze how distributed Lincoln bearing models behave with very small and very large bearings.

Two cylindrical roller bearings with distributed loading are created in Lincoln, see Table 4.3. Koyo_Cyl_25x47 is chosen as the smallest bearing to reasonably be used in current Volvo applications. Koyo_Cyl_130x340 is bigger than anything currently used. Since the rollers in Koyo_Cyl_130x340 are approximately a factor of 9 times larger than rollers in Koyo_Cyl_25x47, they have different dynamic load ratings [9]. Therefore, the design loads are completely different for each bearing.

Table 4.3: The base dimensions of the two extreme cylindrical roller bearings.

Name	Koyo_Cyl_25x47	Koyo_Cyl_130x340
Bearing Bore [mm]	25.00	130.00
Bearing OD [mm]	47.00	340.00
Bearing Width [mm]	12.00	78.00
No. Elements	13	11
Element Diam. [mm]	5.50	50.00
Pitch Diam. [mm]	36.00	235.00
Element Length [mm]	5.50	50.00
Contact Length [mm]	4.90	46.00
Diam. Clearance [μm]	32.50	82.50
Dynamic Capacity [kN]	14.3	771

By analyzing the bearings models from Lincoln, an evaluation could be made by utilizing corresponding reference models from SABR, see Figures 4.11 and 4.12.

These bearing results are in agreement with the reference results obtained from SABR. However, it is interesting to note that small rollers are slightly more flexible and large rollers a bit stiffer compared to references, cf. Figures 4.11 and 4.12. This is because the stiffness equation of the roller is adjusted to the typical bearing dimensions in Volvo applications. The deviation is small and it would not affect the implementation of most practical applications. The systematic differences between the SABR and Lincoln results mean that it would be straightforward to adjust either bearing model if such extreme bearing dimensions are needed.

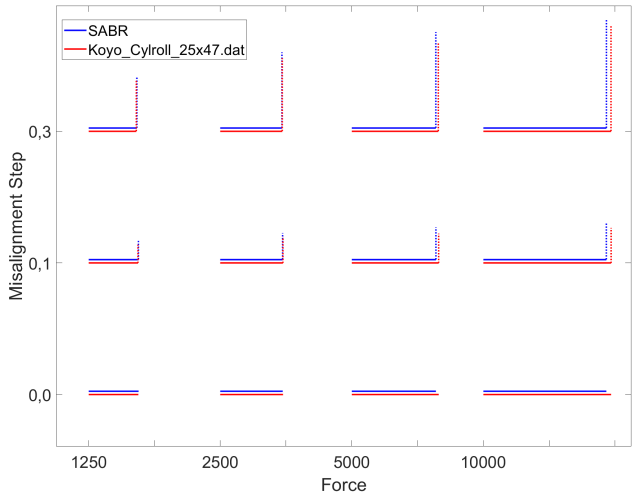

(a)

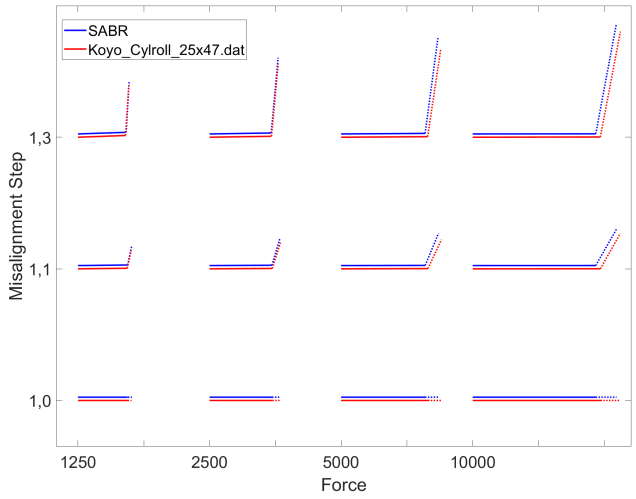

(b)

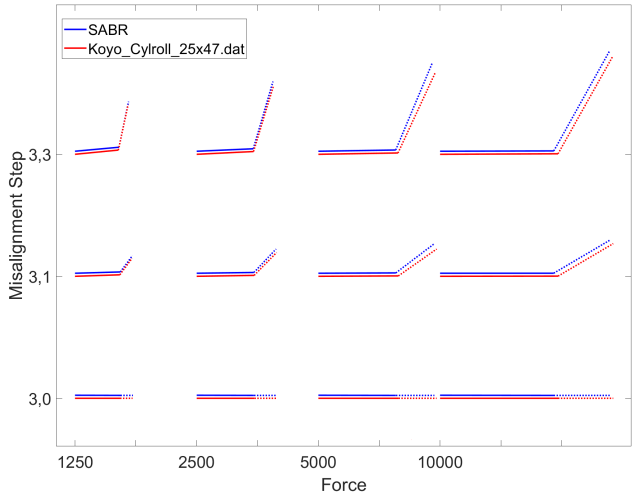

(c)

Figure 4.11: Displacements and reaction moments for different misalignment steps a) 1-3, b) 4-6 and c) 7-9 and different loads. Results obtained from Koyo_Cyl_25x47 and SABR reference.

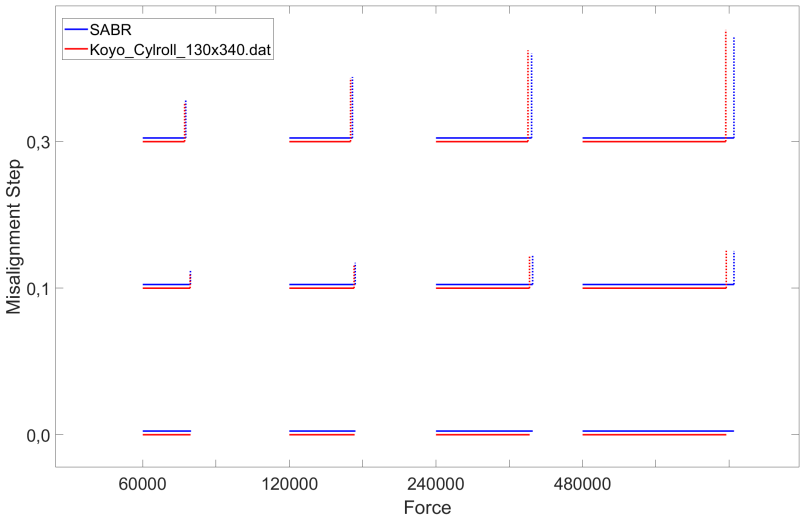

(a)

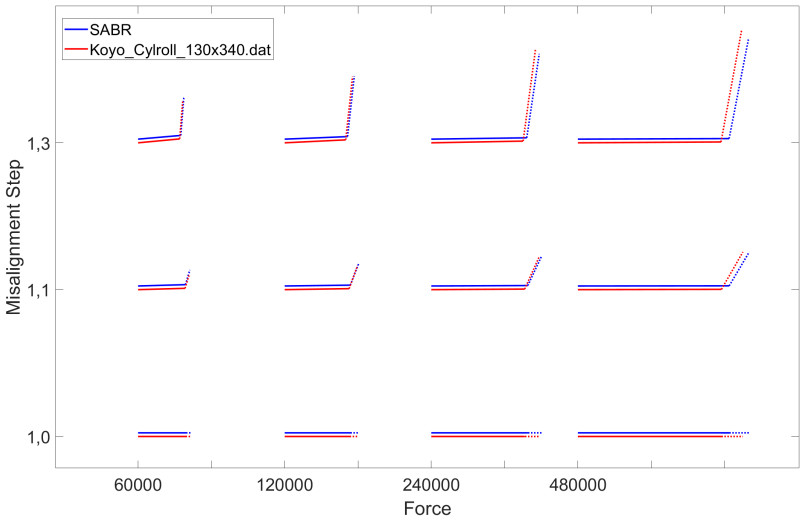

(b)

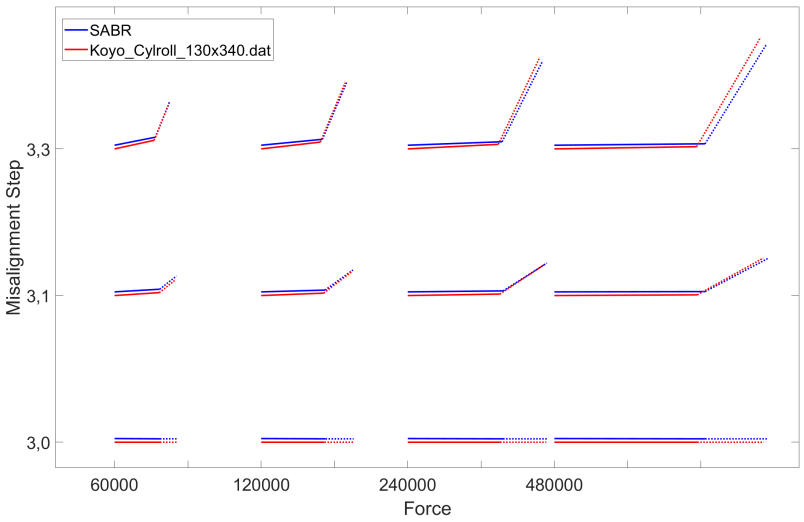

(c)

Figure 4.12: Displacements and reaction moments for different misalignment steps a) 1-3, b) 4-6 and c) 7-9 and different loads. Results obtained from Koyo_Cyl_130x340 and SABR reference.

4.5 Mesh study of discrete bearing model

The purpose of this study is to find out how the mesh of the inner and outer rings affects the stiffness of discrete bearing models. This is done by modifying the elements in the circumferential and radial directions.

As mentioned in Section 2.1, Lincoln has settings for the ring mesh in radial and circumferential direction. It is possible to define the number of element layers in the radial direction and the number of elements between adjacent rollers circumferentially. The relative size difference between adjacent elements in the radial and circumferential direction is adjusted with growth factors, see below [4].

The first sub-study comprised of modification of the elements in the circumferential direction. Two different circumferential growth factors, 1 and 2, are used. The number of elements are chosen so that the smallest elements are of comparable size. Figure 4.13 illustrates the difference. The radial distribution is kept constant with growth factor 1 and 5 elements, excluding the flange. Figure 4.13a shows a discrete bearing with 24 elements per roller and growth factor of 1 for the rings. Figure 4.13b shows a discrete bearing with 8 elements per roller and growth factor of 2 for the rings.

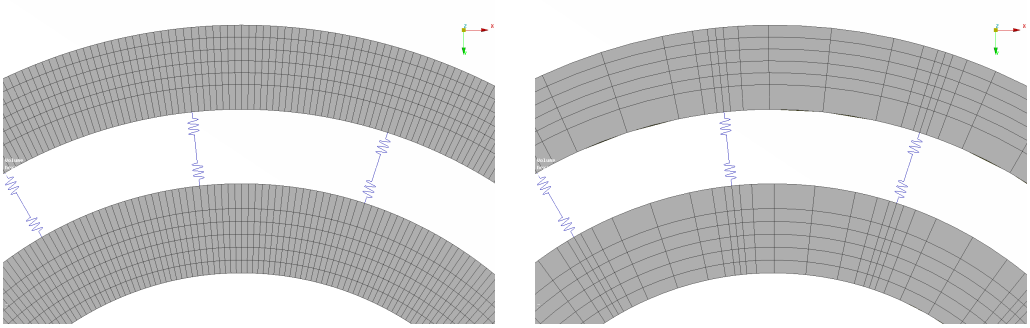

(a) **(b)**

Figure 4.13: Discrete Bearing models with circumferential growth factors a) 1 and b) 2.

Table 4.4 shows the custom ring elements of the discrete bearings in circumferential direction. The setups are chosen in such a way that the smallest element width of growth factor 1 is roughly equal to the smallest element width of growth factor 2.

Table 4.4: Discrete bearings with modified elements between rollers circumferentially for growth Factors (GF) 1 and 2. IR: Inner Ring. OR: Outer Ring.

Elements Circumferentially	
GF = 1	GF = $\sim$ 2
IR=6, OR=8	IR=4, OR=5
IR=12, OR=16	IR=6, OR=7
IR=18, OR=24	IR=7, OR=7
IR=24, OR=32	IR=8, OR=8
IR=33, OR=44	IR=9, OR=9
IR=42, OR=56	IR=10, OR=10

The columns represent bearings with growth factors 1 and 2. Each row corresponds to the elements of inner and outer rings of respective setup. For rings with growth factor 1, the number of elements for the inner ring is three-fourths of the number of elements for the outer ring. As mentioned previously, the setups in each row are correlated so that the smallest element of each bearing is equal.

The following part moves on to describe the second sub-study which comprised of modification of elements in radial direction. Two different circumferential distributions of elements are chosen for this study. The first one has a growth factor of 1 and 12 elements per roller. The second one has a growth factor of 2 and 6 elements per roller. Three different radial modifications are done for each of these two bearings. The inner and outer rings consist of 3, 5 and 8 elements with growth factor 1 in radial direction. Figure 4.14 illustrates the difference between 3 and 5 radial elements. Note that the element layer of the flanges is not counted.

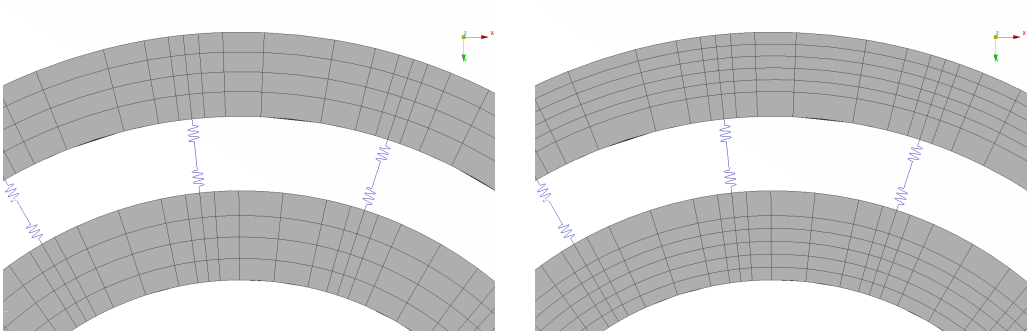

Figure 4.14: Discrete Bearing models with radial elements a) 3 and b) 5. Radial growth factors are 1.

After analyzing the bearings, data were collected and imported into Matlab for evaluation. In Matlab, scripts are created to plot deformation as a function of the size of the smallest element divided by the roller diameter.

Figure 4.15 shows the results of the circumferential modification. From the graph it can be seen that the growth factor does not affect the result since the two curves are roughly equal. However, the size of the smallest element affects the stiffness. It is important to keep in mind that this behavior exists and by choosing a fine mesh, stiffness will change. This is a expected behavior in FEA. Smaller element sizes give more deformation.

Figure 4.16 shows the results of the radial modification. It is notable that the number of elements affects the stiffness; the larger the elements, the bigger their impact on the stiffness. This plot confirms as well that the smallest circumferential element is of importance and not the number of elements. The results of the two lines are matching with the smallest elements being the same.

This study has shown that the overall bearing stiffness changes when modifying the elements distribution of discrete bearings in radial and circumferential direction. The default element was used in earlier work to calibrate the spring stiffness

for discrete models. If other element distributions are used, the stiffness of the bearing will change and the spring stiffness may have to be adjusted.

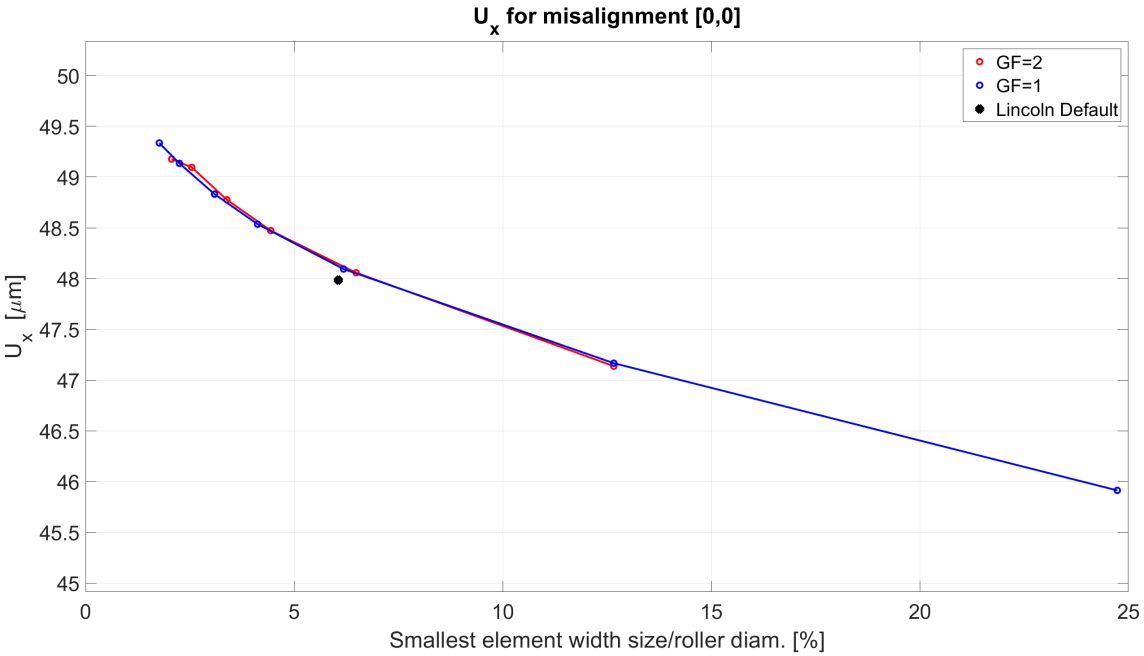

Figure 4.15: Discrete bearings with modified elements in circumferential direction. Blue denotes element configurations circumferentially with growth factor 1. Red denotes element configurations circumferentially with growth factor 2.

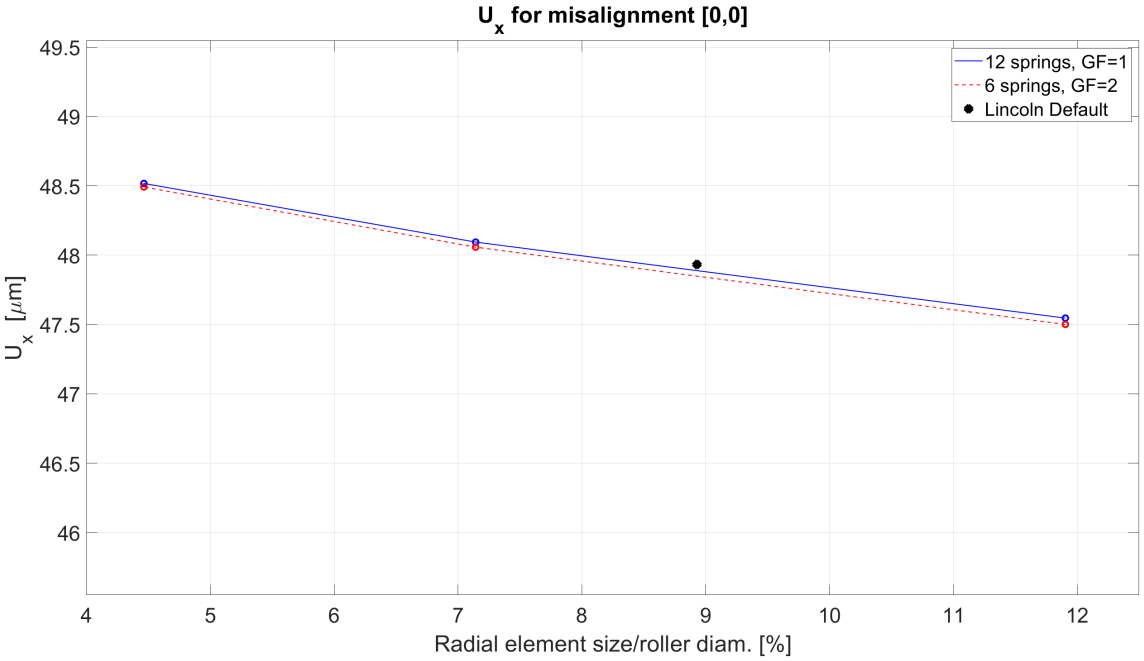

Figure 4.16: Discrete bearings with modified elements 3, 5 and 8 in radial direction. Blue denotes 12 elements per roller for inner ring and growth factor 1. Red denotes 6 elements per roller for inner ring and growth factor 2.

4.6 Investigation of the effect of spring density and surrounding mesh on the response of integrated bearing models

This study was established to investigate how the number of springs along each roller and the number of rows of springs circumferentially that model each roller as well as the mesh of the surrounding parts influence the bearing stiffness of integrated bearings. Inner and outer rings of the integrated bearings are part of the connected parts. For this study several rings meshed with second-order tetragonal elements of different sizes were provided. Hence, only springs are created in Lincoln and connected to the surrounding parts.

This investigation consists of three different sub-studies where two integrated bearings are analyzed. The roller bearings are specified in Table 4.1.

In the first sub-study, three integrated models with 6, 12 and 24 springs along each roller are created, see Figure 4.17. Four ring pairs with element sizes 5, 10, 20 and 30 % of the roller diameters are provided for each bearing. Figure 4.18 illustrates the difference between mesh sizes 5 and 20 percent of the roller diameter of Koyo_Cylindrical_30x90. For both bearings all combinations of ring and roller models are analyzed with ten increasing load levels. There is no misalignment applied.

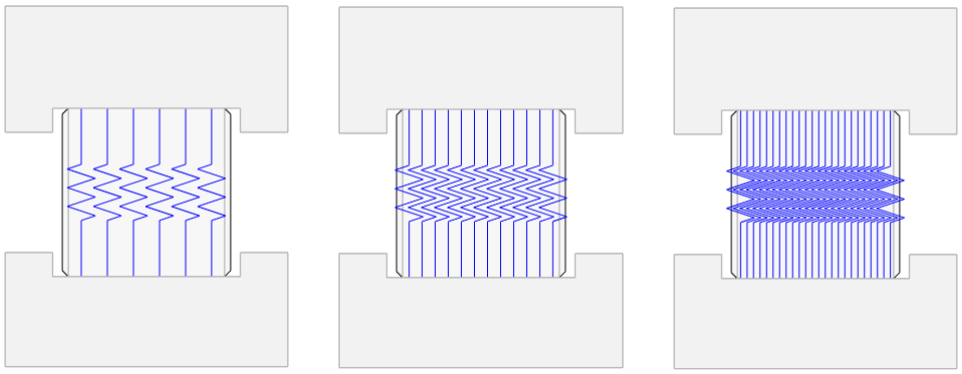

(a) 6 springs **(b)** 12 springs **(c)** 24 springs

Figure 4.17: Number of springs that models each roller axially.

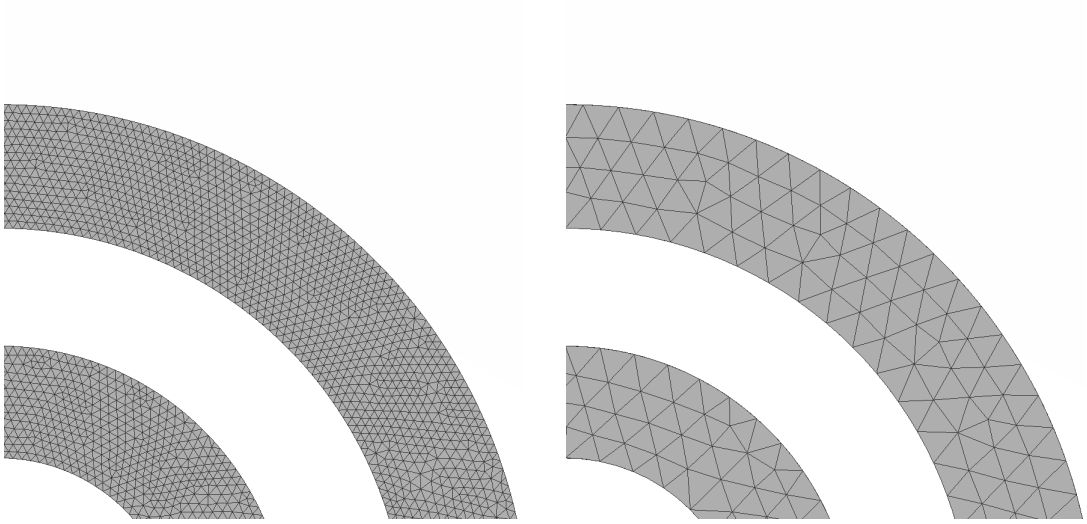

(a) 5 % **(b)** 20 %

Figure 4.18: Tetragonal meshes for the rings of Koyo_Cylindrical_30x90.

Figures 4.19 and 4.20 show the results for Koyo_Cylindrical_30x90 and Koyo_Cylindrical_50x90 with radial deformation as a function of radial force. Element sizes are differentiated by colors. For each spring configuration, the four mesh sizes with 5, 10, 20 and 30 % of the roller diameters are compared.
For Koyo_Cylindrical_30x90, the element sizes are 0.75, 1.5, 3.0 and 4.5 mm. For Koyo_Cylindrical_50x90, the element sizes are 0.5, 1.0, 2.0 and 3.0 mm. These findings show that with increasing spring density, stiffness increases. As element size decreases, flexibility increases. However, the stiffness difference between element sizes becomes smaller as the spring density increases. By studying the force levels separately, it can be seen that the stiffness difference between element sizes increases when the load increases.

Figure 4.21 compares the results by plotting deformation of one load level. There are 2 springs between adjacent rollers circumferentially. The bearings have different spacings. That is, the distance between springs divided by roller diameter is different for the bearings. It is evident that there is a limit beyond which more springs do not affect the stiffness. It can also be seen that larger spacing leads to divergent behavior. The curves are inclined which means that there is an effect of element size that remains.

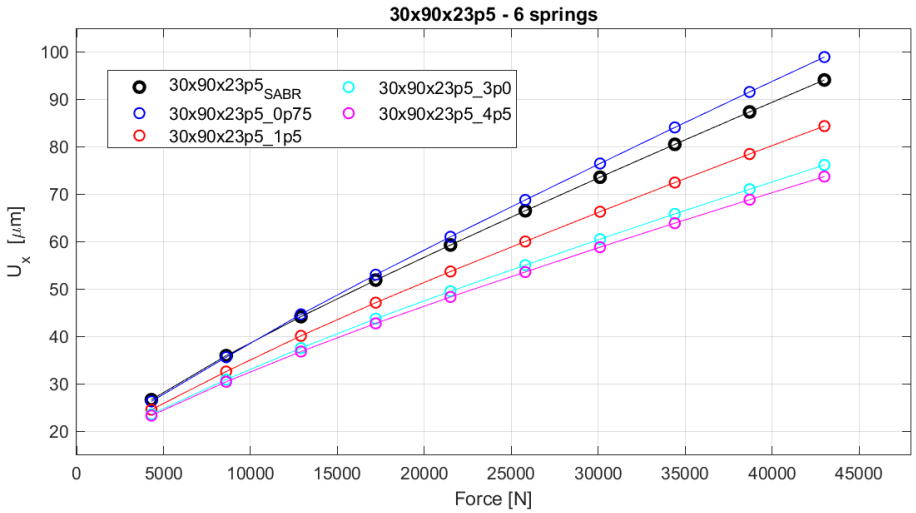

(a)

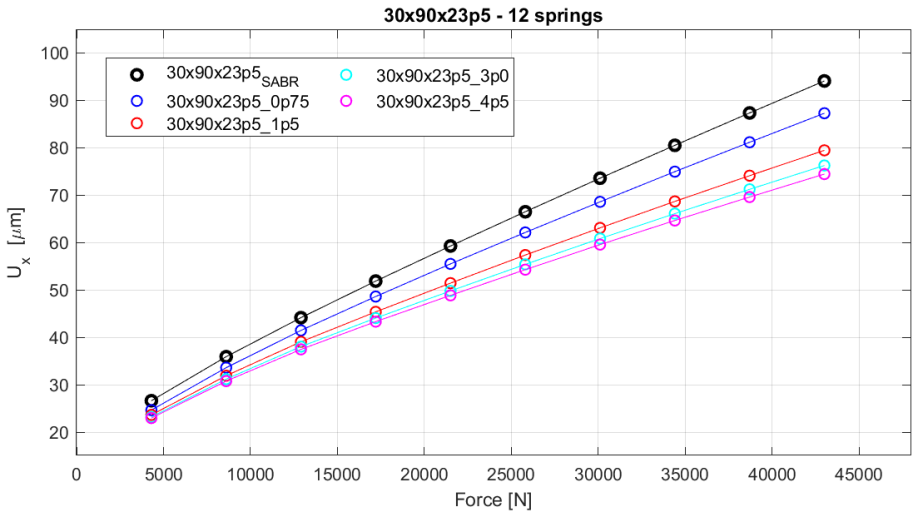

(b)

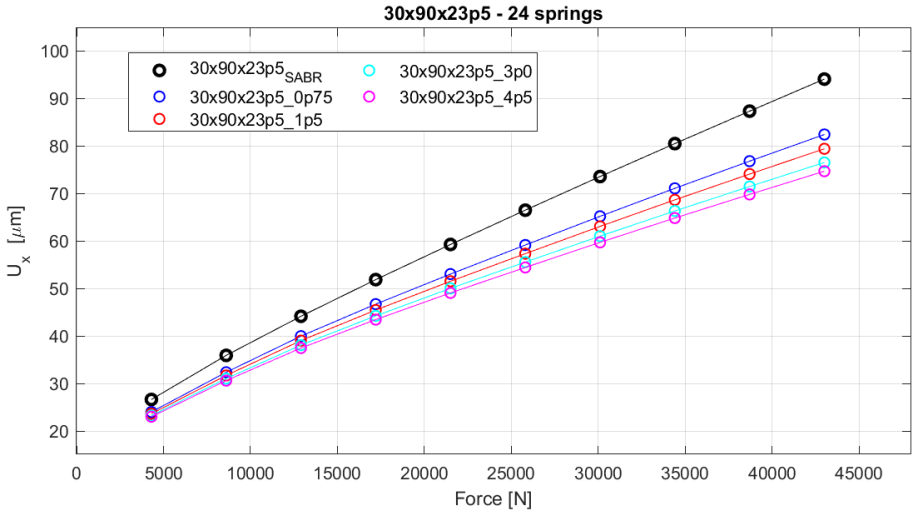

(c)

Figure 4.19: Integrated Koyo_Cylindrical_30x90 bearings of a) 6 b) 12 and c) 24 springs along each roller. Element sizes consist of 0.75, 1.5, 3.0 and 4.5 mm.

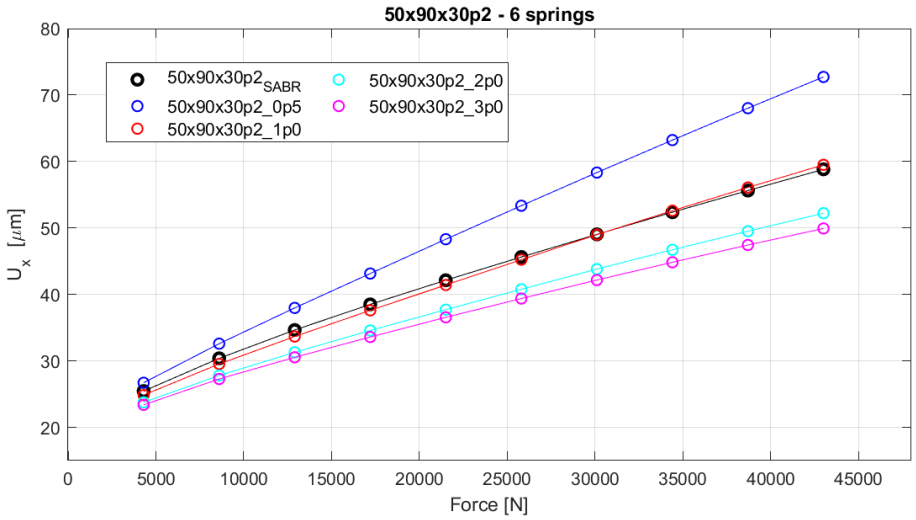

(a)

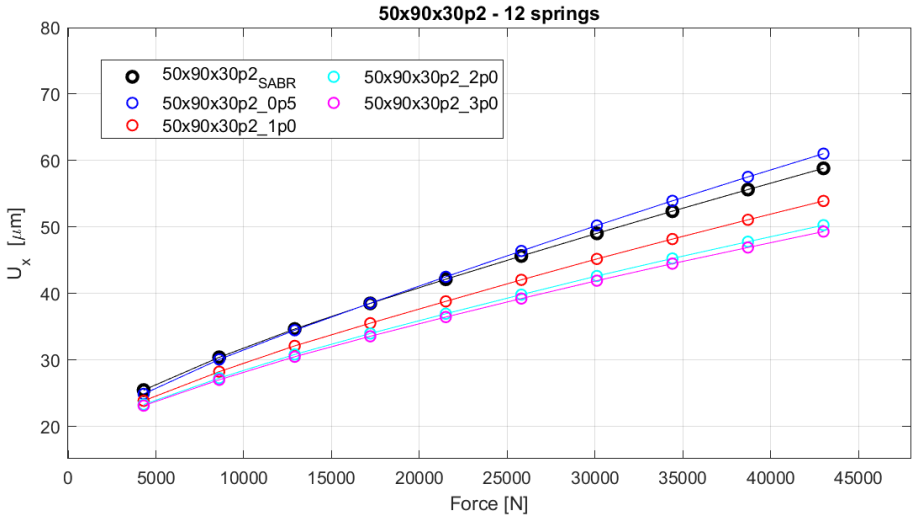

(b)

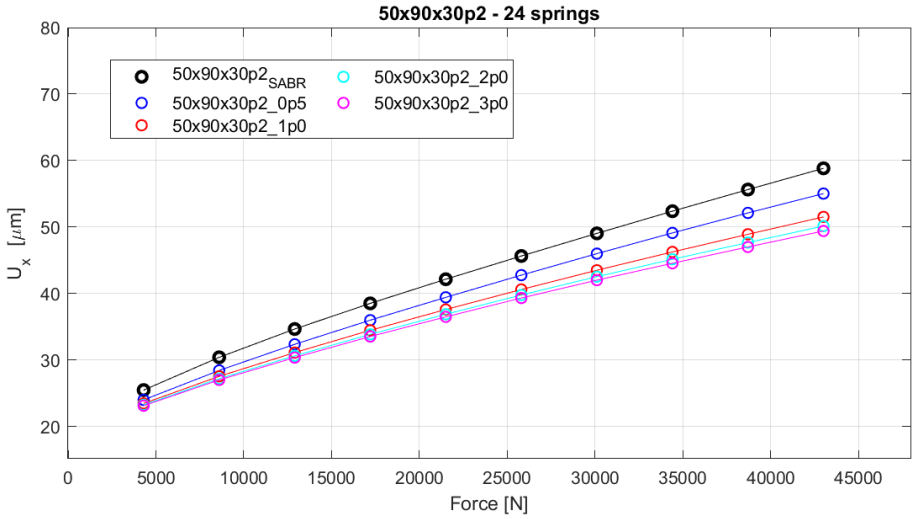

(c)

Figure 4.20: Integrated Koyo_Cylindrical_50x90 bearings of a) 6 b) 12 and c) 24 springs along each roller. Element sizes consist of 0.5, 1.0, 2.0 and 3.0 mm.

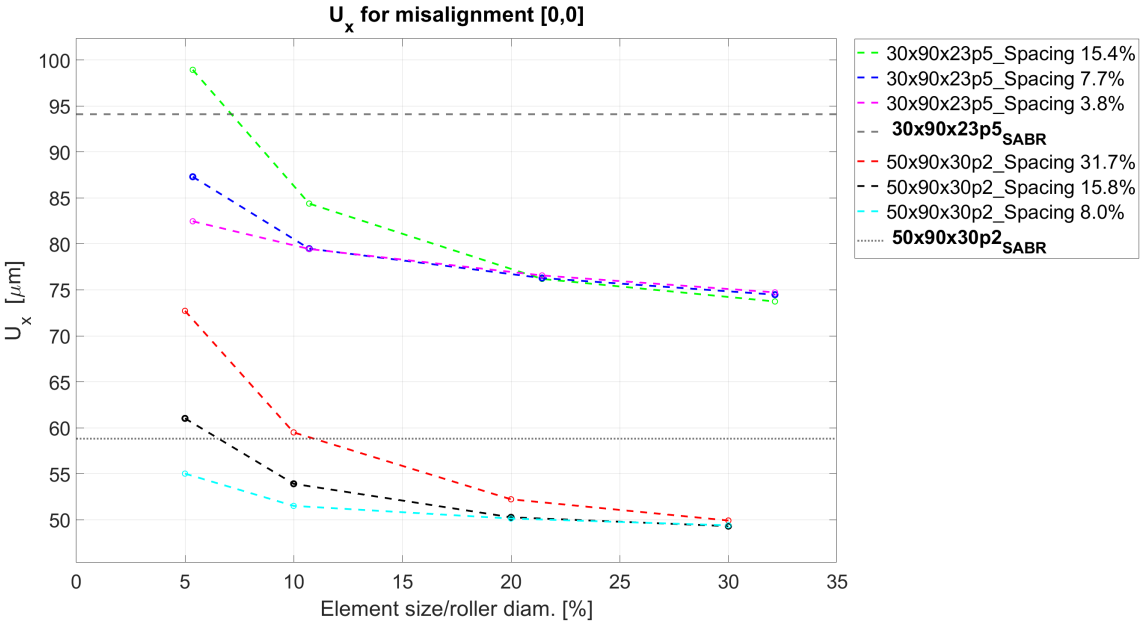

Figure 4.21: Integrated bearing models Koyo_Cylindrical_30x90 and Koyo_Cylindrical_50x90 with element sizes 5, 10, 20 and 30 % of roller diameter. Number of springs along roller are differentiated by colors.

In the second step of this investigation, three different number of rows of springs in the circumferential direction are used to model each roller. They are selected in such a way that the spring density is equal in both axial and circumferential directions as shown in Figure 4.22. For Koyo_Cylindrical_30x90 6, 12, and 24 rows are selected, see Figure 4.23. The number of spring rows for Koyo_Cylindrical_50x90 are 3, 6 and 12.

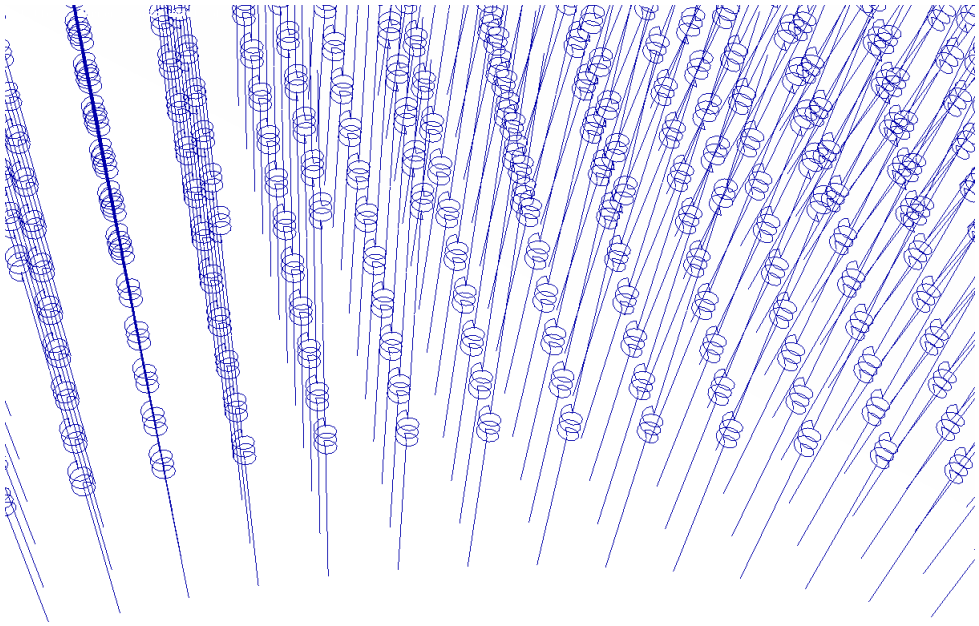

Figure 4.22: Koyo_Cylindrical_30x90 with 3.8 % circumferential spacing for the springs on the inner ring. The spring density is roughly equal in both axial and circumferential directions.

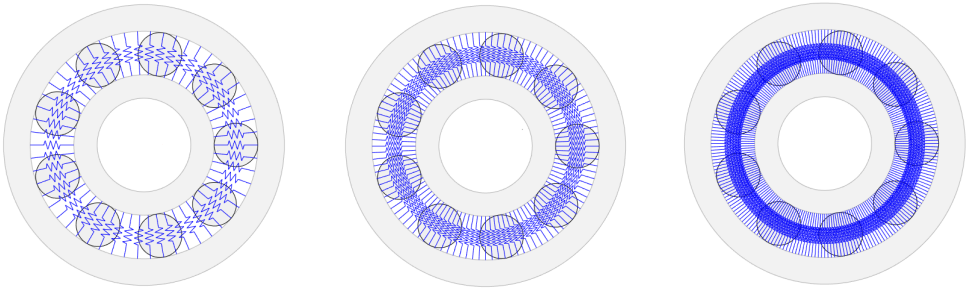

(a) 6 springs per roller **(b)** 12 springs per roller **(c)** 24 springs per roller

Figure 4.23: Number of rows of springs circumferentially that model each roller.

To understand how the circumferential spacing affect the stiffness, deformation is plotted as a function of element size divided by roller diameter, see Figure 4.24. The combinations of numbers of springs along the roller and numbers of rows of springs circumferentially are differentiated by colors.

The results show that increasing spacing in circumferential direction increases the stiffness, cf. Figure 4.21. It can be seen that when element size is larger than the distance between the springs, the resulting stiffness is constant. This means that there are enough springs.

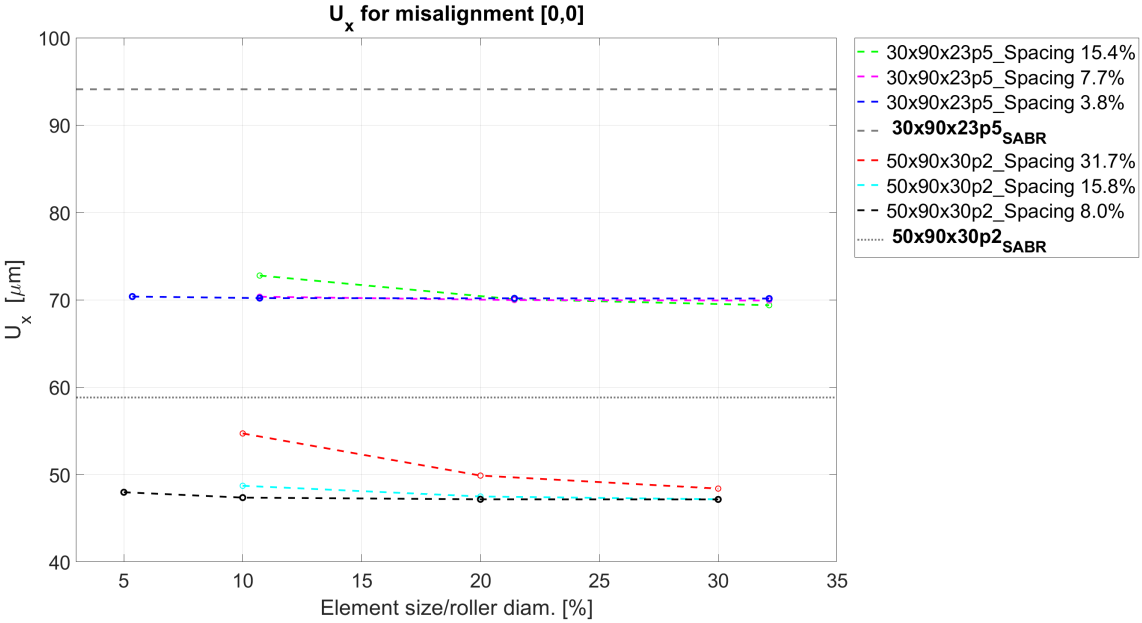

Figure 4.24: Integrated bearing models Koyo_Cylindrical_30x90 and Koyo_Cylindrical_50x90 with element sizes 5, 10, 20 and 30 % of roller diameter.

Previous research has by trial and error established numerical values for the constant C in distributed bearing models, c.f. Section 2.4. In this third sub-study, the aim was to calibrate the stiffness of the rollers, i.e. by trial and error find a constant value of the roller stiffness of the integrated bearings that is close to the reference models.

Based on results from Figure 4.24, an element size of approximately 20 % of the roller diameter is used. The corresponding spring element distance, axial and circumferential, of 80 % of the element size is used. The stiffness constant C of the distributed bearing model is gradually modified in Lincoln and compared with the reference model.

The results of the calibration steps are compared in Matlab, see Figures 4.25 and 4.26. Constant values for the roller stiffness are differentiated by colors.

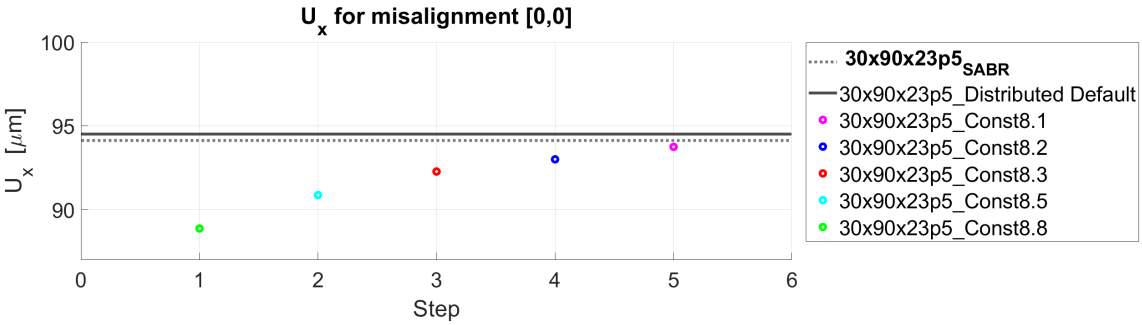

Figure 4.25: Constant C values of the roller stiffness calibrated for Koyo_Cylindrical_30x90. Convergence is obtained after five modifications.

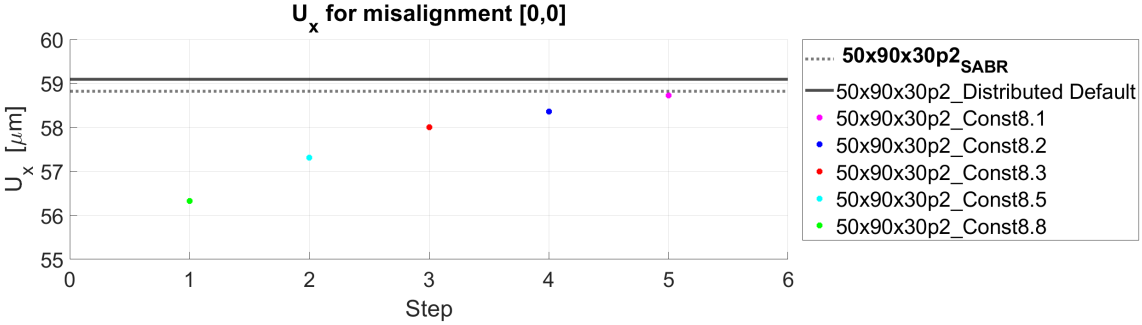

Figure 4.26: Constant C values of the roller stiffness calibrated for Koyo_Cylindrical_50x90. Convergence is obtained after five modifications.

It is clear that when $C = 8.1$, the models are in best agreement with SABR and close to the default stiffness settings for the distributed bearing model. This means that the default distributed stiffness settings in Lincoln can be used for integrated bearings.

The integrated Lincoln bearings are analyzed with distributed roller stiffness parameters and with an element size of 20 % of the roller diameter. Figures 4.27 and 4.28 illustrates the evaluation of the integrated bearings. Results from the bearings are in agreement with the references from SABR. However, by a closer comparison it is evident that integrated models are slightly stiffer than references from SABR.

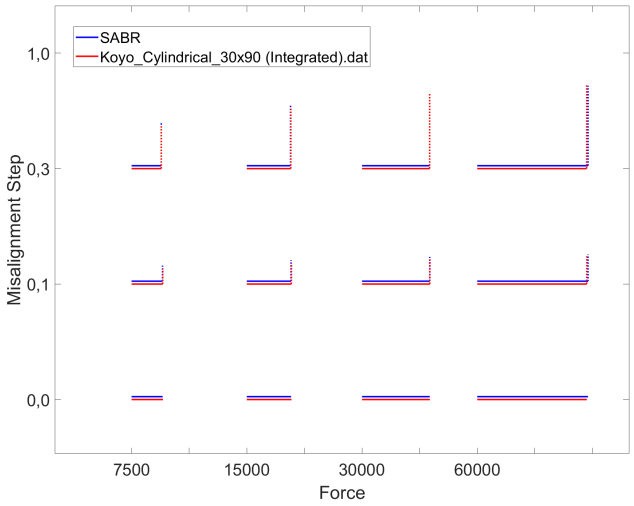

(a)

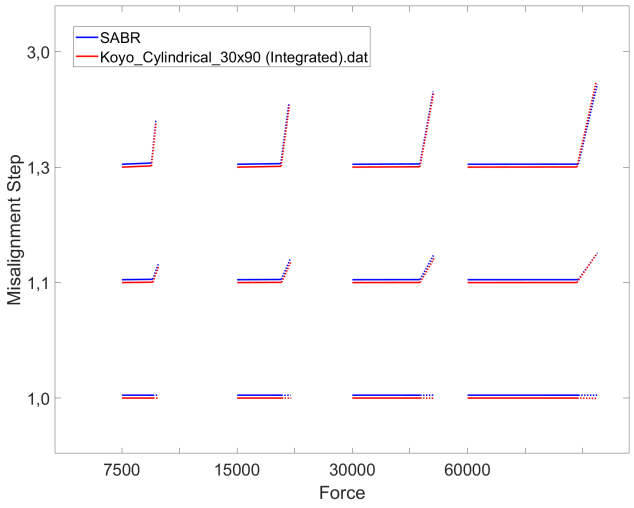

(b)

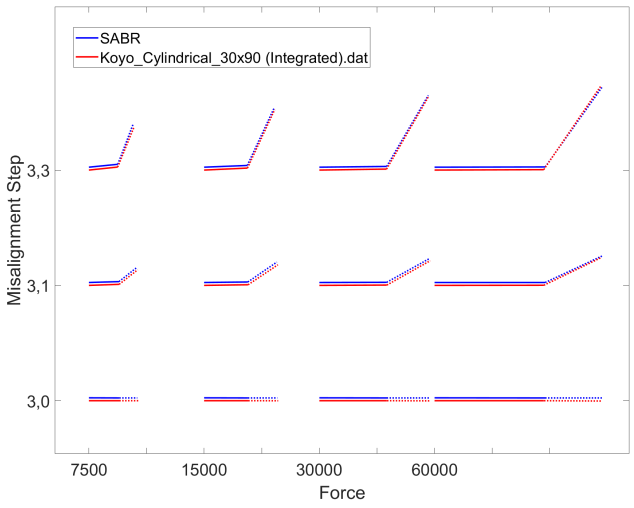

(c)

Figure 4.27: Displacements and reaction moments for different misalignment steps a) 1-3, b) 4-6 and c) 7-9 and different loads. Results obtained from Integrated Koyo_Cylindrical_30x90 and SABR.

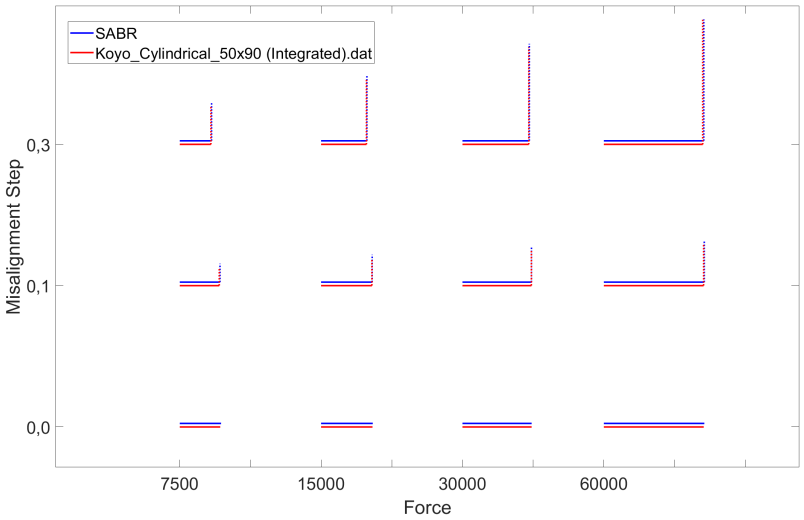

(a)

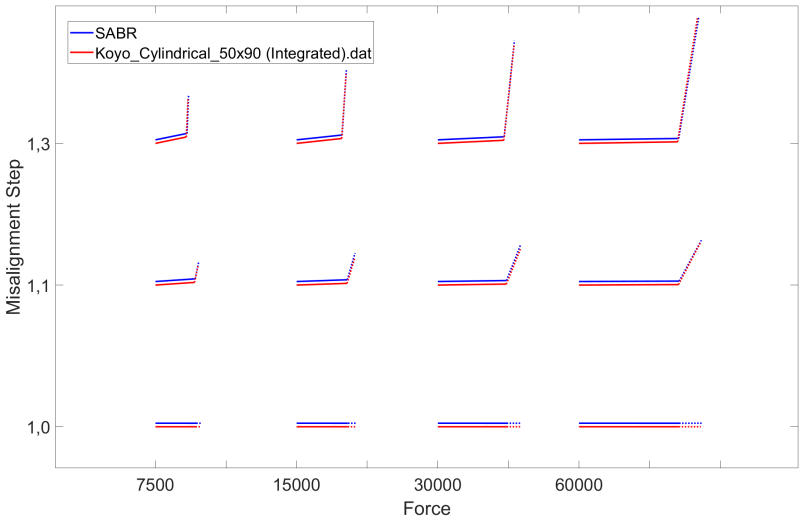

(b)

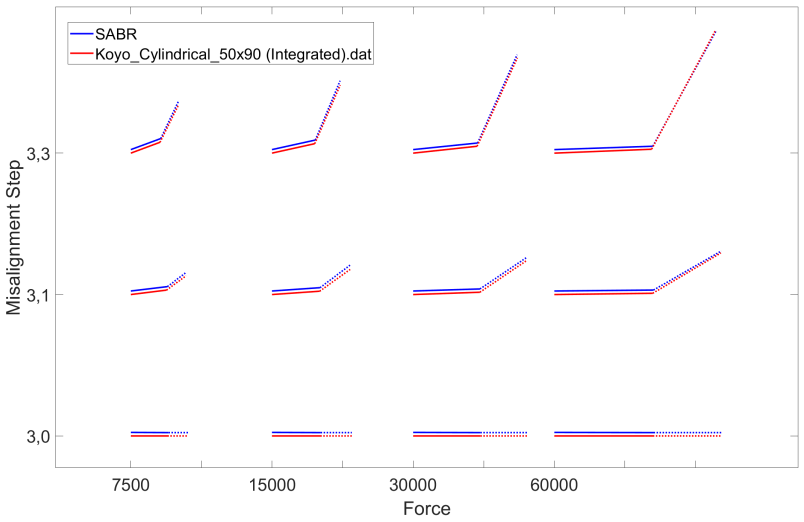

(c)

Figure 4.28: Displacements and reaction moments for different misalignment steps a) 1-3, b) 4-6 and c) 7-9 and different loads. Results obtained from Integrated Koyo_Cylindrical_50x90 and SABR.

4.7 Investigation of axial forces for distributed bearing models

This study has the purpose to find out if the current implementation of axial forces in the cylindrical roller bearing model is sufficiently accurate.

An axially loaded cylindrical bearing will have compressive forces transmitted in the axial direction in the rollers. The forces are transmitted between opposite flanges in the inner and outer rings, see Figure 4.29 [5].

The different radial position, as seen from the center of the bearing, of the inner and outer rings mean that there will be a tilting torque on the rollers when an axial force is transmitted through the bearing. This is balanced by a shift in the axial distribution of the forces between the rollers and rings [5]. This is modeled in the Lincoln model by two rigid beams and an axial spring, see Figure 4.29.

The axial beam is connected to the springs that represent the roller in such a way that the tilting torque mentioned previously can be reacted by the radial forces in the roller. One end of it is in contact with the outer ring flange via the axial spring. The other end is rigidly connected to a radial beam that connects to the opposite flange of the inner ring [5].

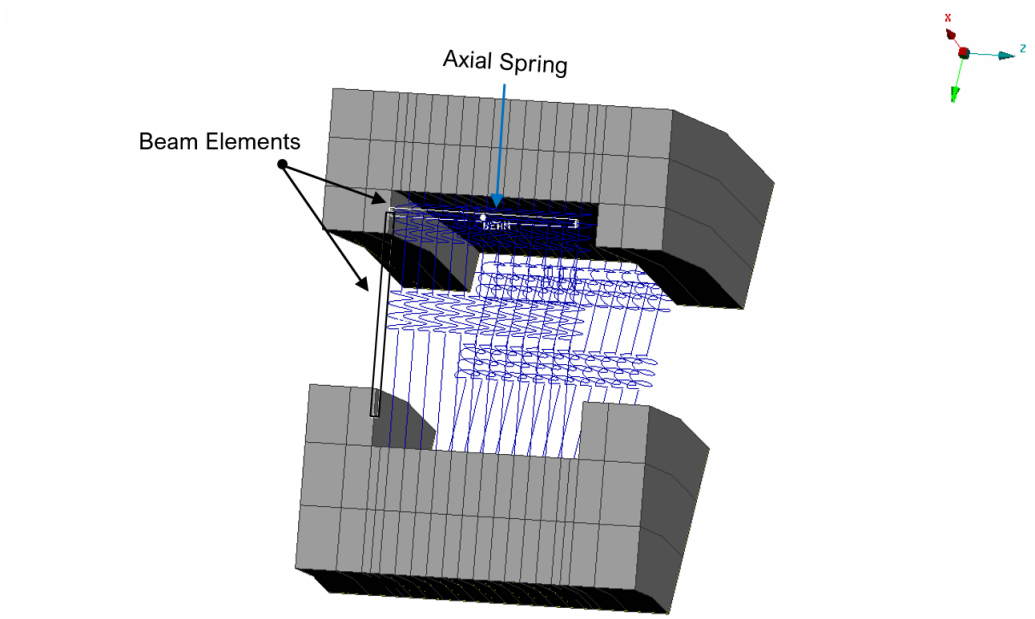

Figure 4.29: Cross section of cylindrical roller bearing where an axial spring is in contact with the flanges of the outer ring. The rigid beam elements connects inner and outer rings.

Two cylindrical roller bearings from Lincoln with distributed loading are used in this study. Koyo_Cylindrical_30x90 is the first one, see Table 4.2 for details. The dimension of the other bearing, Koyo_Cyl_40x90, is detailed in Table 4.5.

Table 4.5: The base dimensions of the cylindrical roller bearings Koyo_Cyl_40x90.

Name	Koyo_Cyl_40x90
Bearing Bore [mm]	40.00
Bearing OD [mm]	90.00
Bearing Width [mm]	33.00
No. Elements	12
Element Diam. [mm]	12.00
Pitch Diam. [mm]	65.60
Element Length [mm]	18.00
Contact Length [mm]	17.00
Diam. Clearance [μm]	37.50
Dynamic Capacity [kN]	822

In this investigation the commercial software SABR is not used as source of reference. This is because the software does not allow for axial forces in cylindrical roller bearings. As a substitute, the commercial software Romax Nexus is used to create the reference models. Romax is a similar software to SABR but it can take axial forces in cylindrical roller bearings into account [10].

The misalignments in this study consist of six different parallel and orthogonal combinations, see Table 4.6. These together with force levels based on the dynamic load rating add up to 84 load-cases for each bearing. Out of these, there are 18 purely radial forces and 18 purely axial forces. The remaining 48 consist of combinations of radial and axial forces.

Table 4.6: The combined misalignments that are used with radial, axial and combined radial and axial loads.

Misalignment step	1	2	3	4	5	6
Parallel [mrad]	0	0	0	2	2	2
Orthogonal [mrad]	-2	0	2	-2	0	2

Axial play has to be manually modified in order to calibrate the response with respect to the reference models. In Figure 4.30 three different models of Koyo_Cyl_40x90 with axial plays 8, 10 and 14 µm are evaluated for four purely axial loads. In this figure, the axial loads of 100, N 6165 N, 12330 N and 24660 N are used for the second misalignment step. As seen the play affects the deflection. The axial play 10 µm is in agreement with the reference model, when observing the force at the lower force of 100 N.

The axial stiffness of the rollers is calibrated with a reference model from Romax. Figure 4.31 shows three different stiffness configurations of Koyo_Cyl_40x90. It is clear that the axial stiffness should be high and does not give a significant contribution to the total deflection.

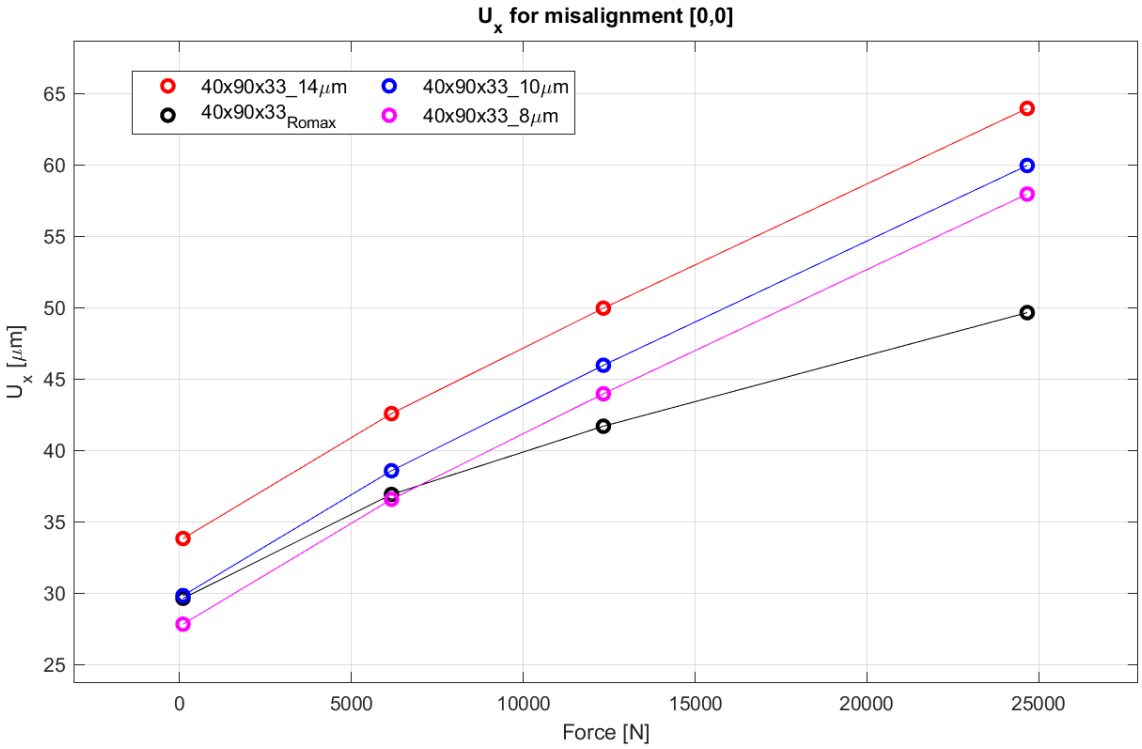

Figure 4.30: Selecting the axial play parameter that gives the best response for Koyo_Cyl_40x90. The axial loads are 100 N, 6165 N, 12330 N and 24660 N.

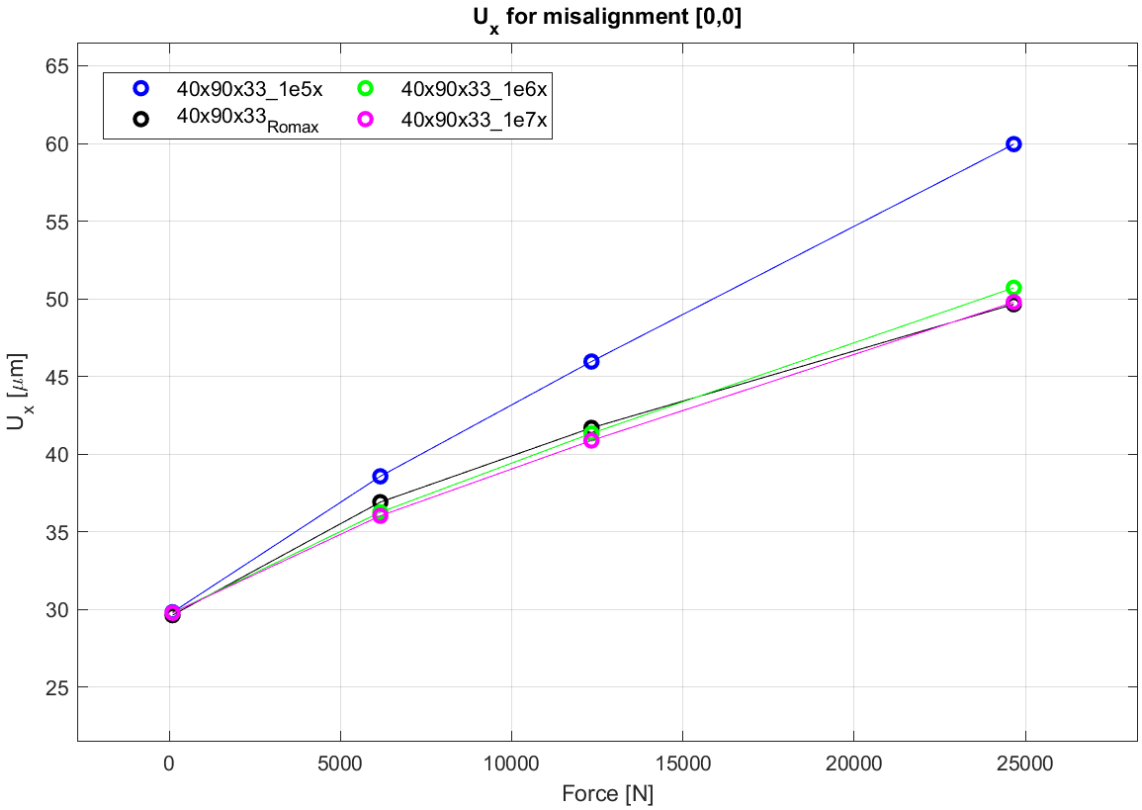

Figure 4.31: Calibration of axial stiffness for Koyo_Cyl_40x90. The axial loads are 100 N, 6165 N, 12330 N and 24660 N.

When axial play and stiffness were calibrated for the two bearings, the main evaluation could be done by analyzing all the 84 load cases. Figures 4.32 and 4.33 displays the results for Koyo_Cylindrical_30x90. Besides displacement in radial and axial (x and z) direction, the displacements in y-direction (orthogonal out of plane), are shown with half circles in Figure 4.33 in which the load cases with parallel misalignment is shown. Results for Koyo_Cyl_40x90 are shown in Figure 4.34 and Figure 4.35.

From the below figures it is evident that the distributed bearings from Lincoln can model pure axial loads and combined loads (radial and axial) in a good way. When looking in detail at the higher axial loads, it is found that there is some deviation for the reaction moments. Cylindrical roller bearings are not intended to be used unless the radial force is larger than the axial force. Thus, these differences are not important. Nevertheless, if such an implementation is done in the future, care should be taken.

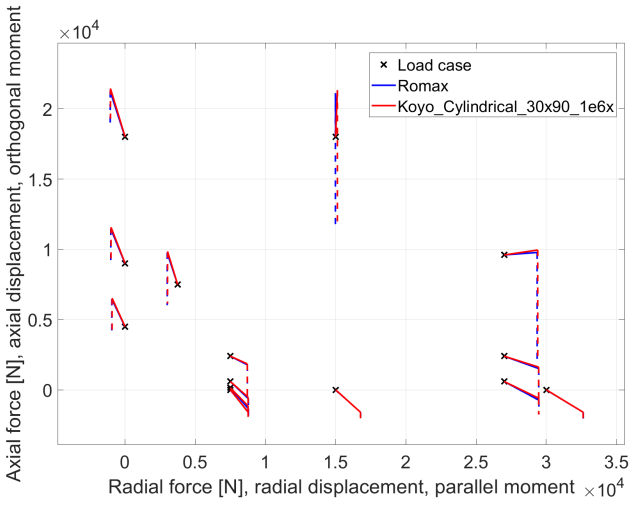

(a)

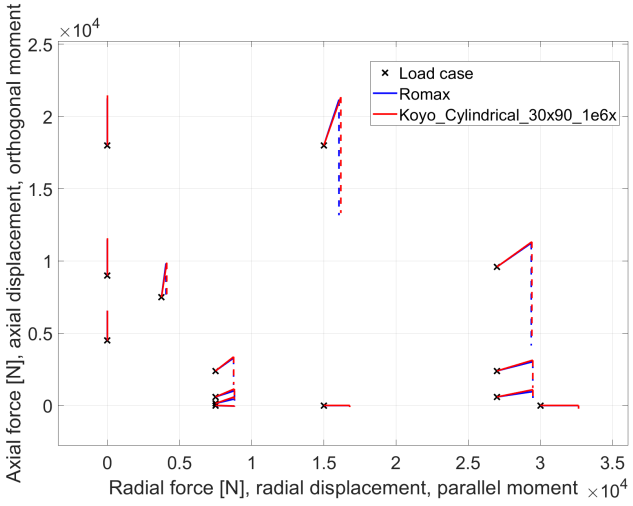

(b)

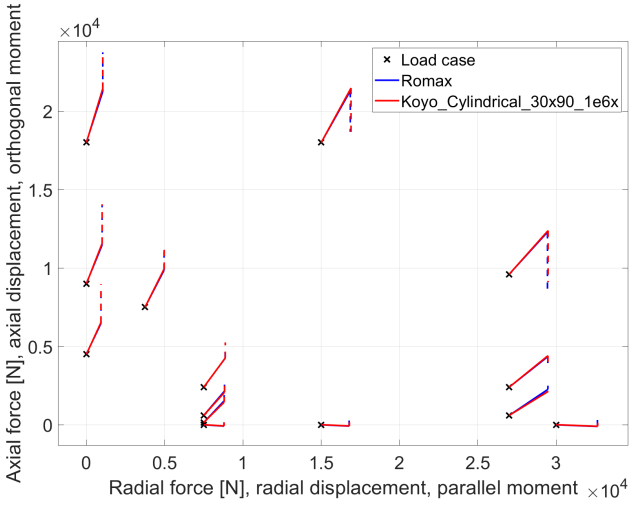

(c)

Figure 4.32: Displacements and reaction moments for different misalignment steps a) 1, b) 2 and c) 3 and different loads. Results obtained from Distributed Koyo_Cylindrical_30x90 and Romax.

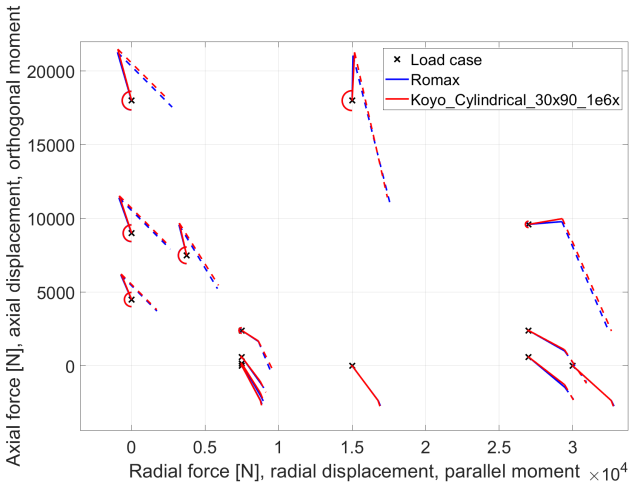

(a)

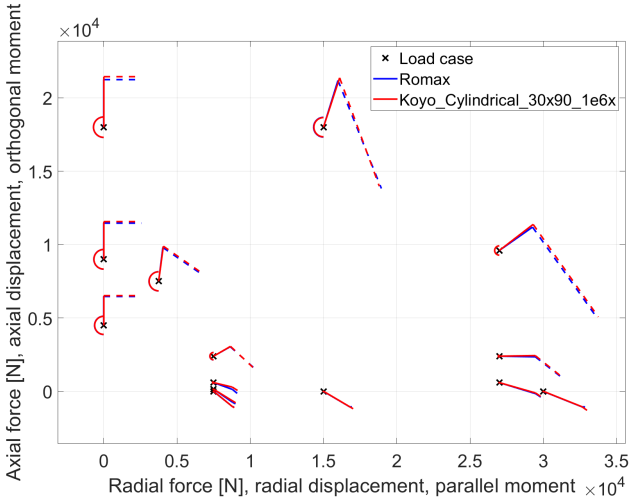

(b)

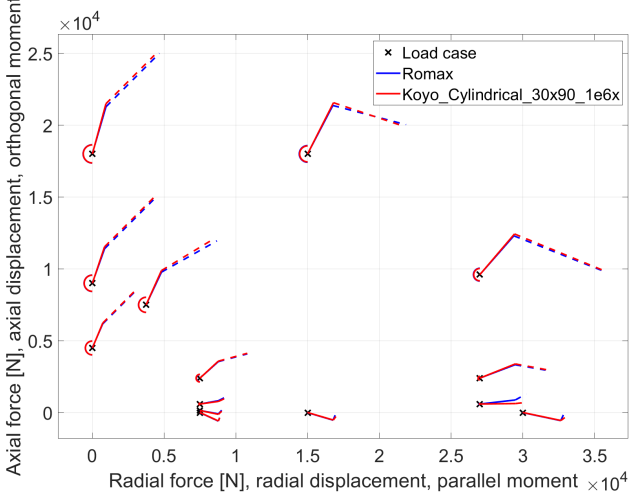

(c)

Figure 4.33: Displacements and reaction moments for different misalignment steps a) 4, b) 5 and c) 6 and different loads. Results obtained from Distributed Koyo_Cylindrical_30x90 and Romax.

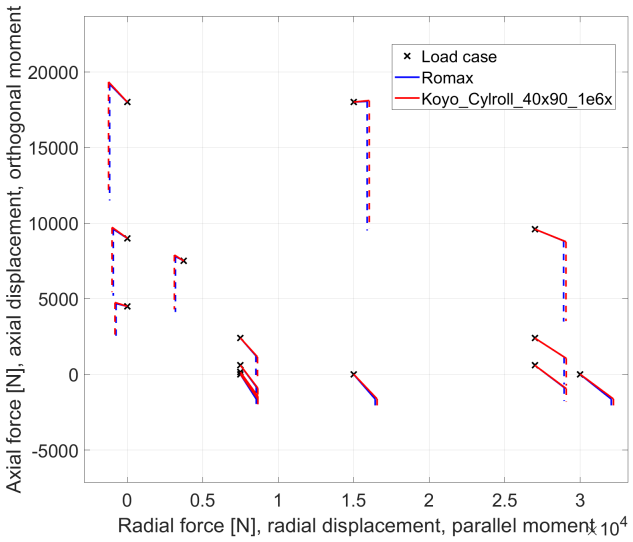

(a)

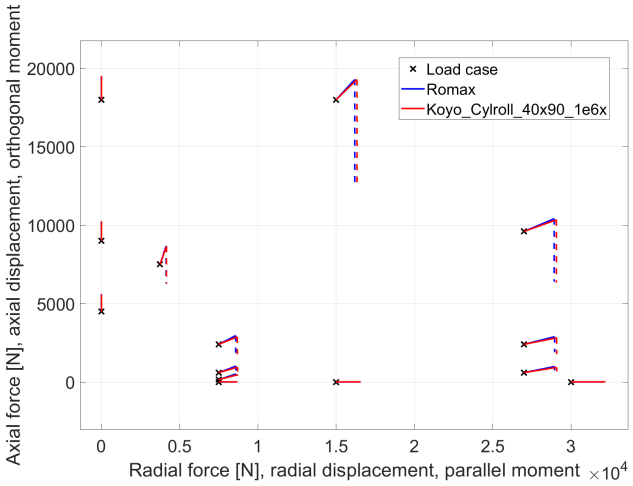

(b)

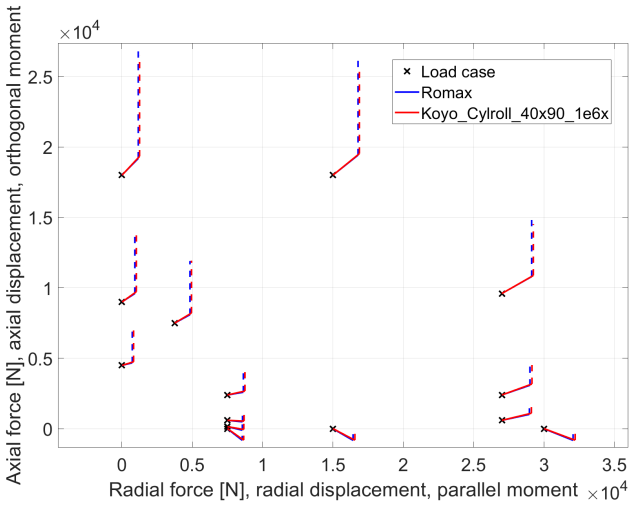

(c)

Figure 4.34: Displacements and reaction moments for different misalignment steps a) 1, b) 2 and c) 3 and different loads. Results obtained from Distributed Koyo_Cyl_40x90 and Romax.

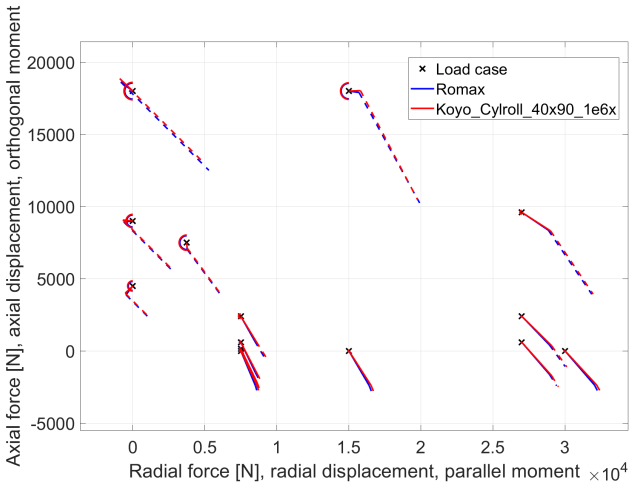

(a)

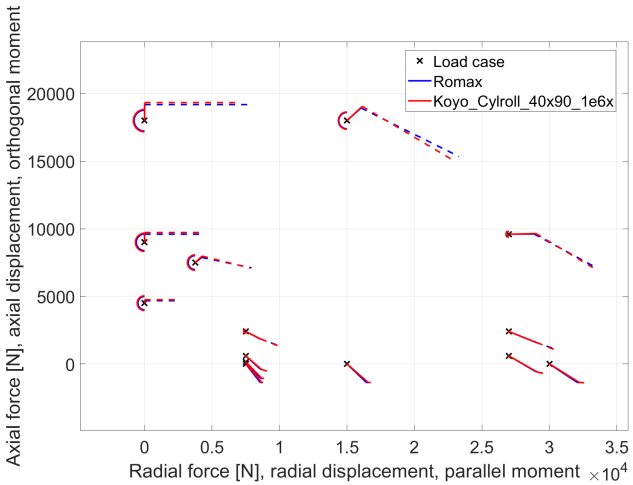

(b)

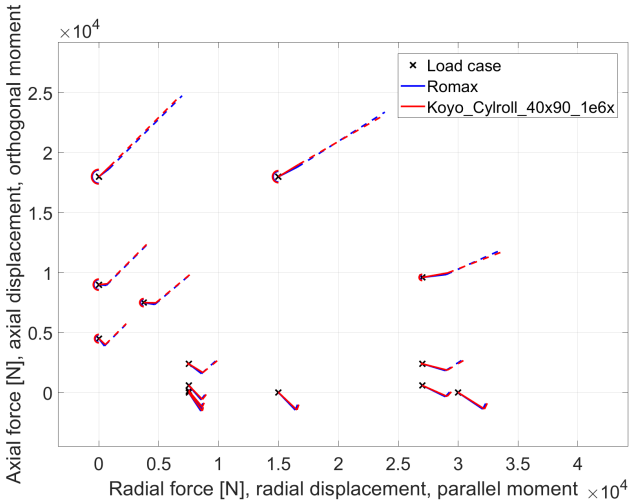

(c)

Figure 4.35: Displacements and reaction moments for different misalignment steps a) 4, b) 5 and c) 6 and different loads. Results obtained from Distributed Koyo_Cyl_40x90 and Romax.

5
Discussion

5.1 Replacement of non-linear springs with gap elements in roller-modelling

The current models, both distributed and discrete for Model O, implements non-linear spring elements and are usable in FE analyzes but are not as stable as desired. Volvo's experience has shown that gap-elements are more resource-efficient and more stable than nonlinear springs in large FE models. To implement gap elements, it is necessary to ensure that the modified model converges and that the results are similar to these of as Model O. This is confirmed in the study in Section 4.1. The new model with gap-elements is expected to require less computational time than the present models based on Volvo's experience. This however needs to be confirmed in larger assemblies.

5.2 Stiffness of integrated rings and observed difference between needle and roller bearings

Prior studies have shown an apparent stiffness difference between cylindrical roller bearings and needle roller bearings. It can from the study in Section 4.3 be seen that by changing the ring thickness, Lincoln (FE) models give reasonable changes in stiffness, i.e., thicker rings become more flexible. On the contrary, SABR's reference models ignore the thickness of the rings. Instead, tolerance (effective clearance) changes, resulting in unreasonable results if this is not understood. In Section 4.4 large and small bearing sizes, are evaluated. It is shown that the developed model gives reasonable results. Thus, with proper attention to bearing play it is expected that both cylindrical roller and needle bearings are correctly modelled.

Integrated loading models are common for needle bearings. To be able to get reliable needle bearing models, it is important to know how to distribute elements and springs. This is clarified in Section 4.6 where a dimensional threshold is determined. That is, when the element size is equal to or larger than the spring spacing, the model shows a stable behavior.

5.3 Mesh influence of discrete bearing models

In the course of modelling discrete bearings in Lincoln, the simplification study in Section 4.2 was discovered. This investigation shows that the very thin elements directly under the rollers can be removed without affecting the results. The simplification was unexpected but important for following bearing analyzes as it decreases the computing time. The local stress difference that occurs due to this modification is irrelevant for components such as shafts or housing that are of interest in this case.

The mesh study in Section 4.5 shows that the stiffness in bearings is dependent on radial and circumferential element distributions to some extent. But it also shows that the default element sizes and the stiffness of the springs conform.

5.4 Distributed bearing models

The objectives of this thesis work do not include studies for distributed bearing models. However, this became relevant later on in Section 4.3 when comparing ring thicknesses. From Figure 4.9 it can be seen that the distributed and discrete bearings differ for very thin bearing rings. A further study with more focus on this could be relevant.

In 4.6 the stiffness of rollers for the integrated bearing models are calibrated. Figures 4.25 and 4.26 visualizes this in detail. These figures show that the default stiffness parameters for the distributed bearing model conform to those of SABR. This indicates that the calibration for the distributed models is reliable and can be used to validate bearings of typical dimensions in Volvo applications.

5.5 Investigation of axial forces for distributed bearing models

In this investigation, it was evident that multiple runs are necessary to calibrate axial stiffness and axial play. Further research should be undertaken to investigate the possibility to calibrate from existing data to avoid extra analyzes.

The stiffness of the axial springs are much higher than the stiffness of the radial springs. This means that there is no requirement to use axial springs in the rollers. In future investigations, it might be possible to use a different element instead for the spring.

6
Conclusions

The aim of this thesis was to accurately describe the average or local behavior of roller bearings and provide finite element results of the desired detail level close to the bearings. In addition, the results of the models had to be validated using the results of dedicated commercial shaft and bearing analysis tools. The objectives consisted of identifying better ways to model the change from contact to play between the rollers and the rings, investigate stiffness of integrated rings and difference between needle and roller bearings, study mesh influence of discrete bearing models and finally study the axial and combined radial and axial forces. The objectives of this thesis are analyzed and covered in six distinctive investigations. The specific outcome of each study is:

The study of the gap element modelling of the roller raceway contact showed the same results as the existing model with non-linear springs. The gap elements can be used.

The stiffness of the Lincoln bearing model shows a physically reasonable dependence on the ring thickness. SABR shows no such effect. It should be noted that the bearing play in SABR changes when the ring thickness is changed.

The stiffness of discrete bearing models is dependent on the element size of rings in radial and circumferential directions. The default element size had been calibrated to give correct results. These data must be interpreted with caution if other values are used.

If the spring density is too small it has an effect on the stiffness of the bearing. When the spring spacing is equal to or smaller than the element size, the bearing stiffness is not affected by the spring spacing or the element size. Same spacing is needed in axial and circumferenial directions. The default stiffness settings for distributed bearing models can be used for integrated bearings.

Discrete bearing models from Lincoln have the ability to sustain axial and combination of radial and axial loads. The axial play of the models has to be calibrated.

In the analysis of extreme bearing sizes, it has been shown that the model provides good results for a large range of bearing sizes. If very accurate results are wanted for extreme sizes it is recommended to check the bearing model with a reference.

7
Future Work

Further modelling in larger bearing assemblies will have to be conducted in order to confirm that the new model with gap-elements is more stable and resource-efficient and hence require less computational time than the present model with non-linear spring elements.

In the investigation of the effect of spring density on the response of integrated bearing models, only distributed behavior was studied. Further research should be carried out to investigate how the spring density affects the bearing stiffness by using a discrete load distribution method, i.e. one row of springs per roller instead of evenly distributed springs. Also, continued efforts are needed to optimize the calibration process of the stiffness of the models.

The studies of this thesis have treated cylindrical and needle roller bearings of various sizes. A natural progression is to analyze ball bearing models. This involves the generalization of a ball bearing model to account for different bearings of different sizes.

Bibliography

[1] Ashwani Kumar, Himanshu Jaiswal, Faraz Ahmad, and Pravin P. Patil. Dynamic vibration characteristics analysis of truck transmission gearbox casing with fixed constraint of vehicle frame based on fea. *Procedia Engineering*, 97:1107–1115, 2014. "12th Global Congress on Manufacturing and Management" GCMM - 2014.

[2] Zhang Yongqi, Tan Qingchang, Zhang Kuo, and Li Jiangang. Analysis of stress and strain of the rolling bearing by fea method. *Physics Procedia*, 24:19–24, 2012. International Conference on Applied Physics and Industrial Engineering 2012.

[3] Harris A. Tedric. *Rolling Bearing Analysis*. John Wiley and Sons, INC., New York, 4th edition, 2001.

[4] Volvo Group Trucks Technology. Lincoln: Matlab gui for bearings, version 2.5, June 2021.

[5] E. Claesson. Modelling of roller bearings in abaqus. M.s. thesis, Chalmers University of Technology, Gothenburg, Sweden, 2014.

[6] SIMULIA. *Abaqus Analysis User's Guide, Version 6.14*. Dassault Systèmes Simulia Corp, United States, 2014.

[7] Ricardo plc. *SABR 2019.1 Shaft and Bearing Analysis Software User Manual*, 2019.

[8] NSK. Technical report. Technical Report CAT. No. E728g, Japan NSK Ltd., 2013. [Online].

[9] SKF. Basic dynamic load rating, c. `https://www.skf.com/group/products/rolling-bearings/principles-of-rolling-bearing-selection/bearing-selection-process/bearing-size/size-selection-based-on-rating-life/basic-dynamic-load-rating-c`. Accessed Jun. 06, 2021. [Online].

[10] Romax Technology. The most complete simulation platform for engineering the next generation of electro-mechanical drive systems. `https://romax.s3.eu-west-2.amazonaws.com/product-flyer/Romax-Nexus-Flyer.pdf`. Accessed Jun. 10, 2021. [Online].

DEPARTMENT OF INDUSTRIAL AND MATERIALS SCIENCE
CHALMERS UNIVERSITY OF TECHNOLOGY
Gothenburg, Sweden
www.chalmers.se

CHALMERS
UNIVERSITY OF TECHNOLOGY